

# **Polymeric Micelles for Ocular Drug Delivery**

# **Polymeric Micelles for Ocular Drug Delivery**

By: Jeffrey Leung, HBSc.

A Thesis  
Submitted to the School of Graduate Studies  
In Partial Fulfilment of the Requirements  
For the Degree Master of Applied Science

McMaster University

© Copyright by Jeffrey Leung, September 2018

Master of Applied Science (2018)  
Chemical Engineering

McMaster University  
Hamilton, ON

Title: Polymeric Micelles for Ocular Drug Delivery  
Author: Jeffrey Leung, HBSc (McMaster University)  
Supervisor: Dr. Heather Sheardown  
Number of pages: ix, 55

## ABSTRACT

Ocular drug delivery to treat diseases of the anterior segment of the eye continues to be a very challenging task. Static barriers include tight junctions of the conjunctiva and dynamic barriers such as the high turnover rate of the tear film contribute to the impenetrable anterior surface. As a result, conventional ophthalmic medication in the form of eye drops is quickly removed and only <5% of the administered dose is efficiently delivered to the anterior tissues. To improve drug delivery into the ocular tissues, we report on a polymeric micelle drug delivery system that may be used to prolong the precorneal residence time of encapsulated drugs. The polymeric micelles were formed from self-assembly of block copolymers composed of poly(L-lactide)-*b*-polyethylene glycol methacrylate (pLA-*b*-pEGMA). Atom transfer radical polymerization was used to synthesize these bottlebrush copolymers to increase hydrophilicity, neutrality, surface density and hydrophobic shielding. The micelles were able to achieve an 80% encapsulation efficiency of Cyclosporine A and sustained a release for up to 30 days. By varying the chain lengths of the pLA and pEGMA blocks, micelle sizes ranging from 60-120 nm with a near neutral surface were explored for mucopenetrating properties. These findings illustrate that micelles can reduce the administration frequency, dosage, and side effects associated with conventional eye drops.

## ACKNOWLEDGEMENTS

I would first like to thank my supervisor Dr. Heather Sheardown for taking me in when I was just a third year undergraduate student. Thank you for your continuous support and guidance throughout the many years I have spent in the lab. With the freedom you provided me, I was able to explore and investigate projects that truly interested me. Looking back from when I first started as a summer student, the advice and confidence you've provided really helped me mature and grow into who I am today.

Next, I would like to thank my parents, my sister Jessica, and my grandparents for their endless love and support. You've taught me to always work hard so that I can have time to relax after. Although it ended up as just working hard all the time, needless to say it has brought me through undergraduate and graduate school. To my grandparents that always asked about when I was coming home, thank you for always making sure I had enough food. I am so grateful to have such a wonderful family and I believe they earned this degree as much as I did.

A huge thank you to the entire Sheardown group, thank you for making my graduate experience so enjoyable and stress free. Special thanks to Alysha for teaching me ATRP, Fei for all the experiments you helped me run, and Naveed for always offering suggestions and helping me with HPLC. This experience would have been a lot more difficult if it weren't for all of you!

Lastly, I would like to thank my amazing girlfriend, Vivian Thai, for being the backbone of my entire journey. Through all the ups and downs, success and failures, highs and lows, thank you for always being right by my side. I really couldn't have done it without you! To my amazing friend and colleague, Mouhanad Babi, I will never forget the struggle we experienced together in undergrad and how close I was to giving up. You were all there to listen to me when I needed you and I am so lucky to have you as my friends.

## TABLE OF CONTENTS

<b>ABSTRACT .....</b>	<b>iv</b>
<b>ACKNOWLEDGEMENTS .....</b>	<b>v</b>
<b>LIST OF FIGURES .....</b>	<b>viii</b>
<b>LIST OF TABLES .....</b>	<b>viii</b>
<b>LIST OF ABBREVIATIONS AND SYMBOLS .....</b>	<b>ix</b>
<b>CHAPTER 1. INTRODUCTION .....</b>	<b>1</b>
<b>1.1 Thesis Objective .....</b>	<b>2</b>
<b>1.2 Thesis Outline.....</b>	<b>2</b>
<b>CHAPTER 2. LITERATURE REVIEW .....</b>	<b>4</b>
<b>2.1 Anatomical and Physiological Barriers .....</b>	<b>4</b>
2.1.1 Tear Film.....	5
2.1.2 External Fibrous Layer .....	6
2.1.3 Middle Vascular Layer .....	7
2.1.4 Internal Nervous Layer .....	9
<b>2.2 Ophthalmic Drug Delivery Methods .....</b>	<b>11</b>
2.2.1 Topical Administration.....	11
2.2.2 Oral Administration.....	13
2.2.3 Subconjunctival Injections.....	13
2.2.4 Intravitreal Injections.....	14
<b>2.3 Polymerization Techniques.....</b>	<b>15</b>
2.3.1 Free Radical Polymerization.....	15
2.3.2 Controlled/Living Polymerization: Atom Transfer Radical Polymerization.....	16
<b>2.4 Polymeric Micelles.....</b>	<b>18</b>
2.4.1 Micelle Formation and Critical Micelle Concentration.....	18
2.4.2 Ocular Delivery Pathways of Micelles.....	19
2.4.3 Micelle Structure .....	20
2.4.4 Drug Release from Polymeric Micelles.....	21
<b>2.5 Interactions with the Mucus Layer.....</b>	<b>23</b>
2.5.1 Mucoadhesion .....	24
2.5.2 Mucopenetration.....	25
<b>2.6 Diffusion Systems .....</b>	<b>27</b>
2.6.1 Multiple Particle Tracking and Mean Square Displacement .....	27
<b>CHAPTER 3. MATERIALS AND METHODS .....</b>	<b>29</b>
<b>3.1 Materials.....</b>	<b>29</b>
<b>3.2 Synthesis of pLA-b-pEGMA.....</b>	<b>29</b>
<b>3.3 Micelle Formation and Characterization .....</b>	<b>30</b>
3.3.1 Micelle Formation .....	30

3.3.2 Dynamic Light Scattering (DLS) and Zeta Potential .....	30
3.3.3 Transmission Electron Microscope (TEM) .....	31
3.3.4 Critical Micelle Concentration (CMC) .....	31
<b>3.4 Cyclosporine A Loaded Micelles and Release .....</b>	<b>31</b>
<b>3.5 Preparation of Artificial Mucus and Characterization.....</b>	<b>32</b>
3.5.1 Artificial Mucus .....	32
3.5.2 Rheological Measurements .....	32
<b>3.6 Micelle Transport Rates in artificial mucus with MPT .....</b>	<b>33</b>
<b>3.7 Statistical Analysis.....</b>	<b>34</b>
<b>CHAPTER 4. RESULTS AND DISCUSSION .....</b>	<b>35</b>
<b>4.1 Copolymer Characterization .....</b>	<b>35</b>
<b>4.2 Micelle Morphology .....</b>	<b>38</b>
<b>4.3 Rheological Characterization of artificial mucus.....</b>	<b>42</b>
<b>4.4 Cyclosporine A Release .....</b>	<b>42</b>
<b>4.5 MPT and Mucopenetration.....</b>	<b>46</b>
<b>CHAPTER 5. CONCLUSIONS .....</b>	<b>49</b>
<b>CHAPTER 6. REFERENCES.....</b>	<b>51</b>

## LIST OF FIGURES

### Chapter 2

- Figure 1.** Anatomy of the human eye. Modified from 1.  
**Figure 2.** Conventional vs. controlled drug release.  
**Figure 3.** Routes of drug administration to the eye. Adapted from 2.  
**Figure 4.** Mechanism of free radical polymerization. Adapted from 22.  
**Figure 5.** Atom Transfer Radical Polymerization mechanism. Adapted from 23.  
**Figure 6.** Drug release mechanism from polymeric micelles. Adapted from 29.  
**Figure 7.** The fate of mucoadhesive and mucopenetrating particles in mucus. Modified from 35.

### Chapter 4

- Figure 1.** Reaction scheme for the synthesis of pLA-*b*-pEGMA block copolymers.  
**Figure 2.** <sup>1</sup>H NMR spectra of the purified pLA-*b*-pEGMA copolymer.  
**Figure 3.** <sup>1</sup>H NMR spectra of the reaction mixture at t=0 hrs. (top) and t=24 hrs. (bottom).  
**Figure 4.** Transmission Electron Micrograph images of pLA-*b*-pEGMA micelles. (a-d) PL10 series: (a)P5, (b)P7, (c)P10, (d)P20. (e-g) PL5 series: (e)P5, (f)P9, (g)P19.  
**Figure 5.** Zeta potential of PLP micelles with increasing pEGMA content. All measurements were prepared in 10 mM NaCl.  
**Figure 6.** Critical Micelle Concentration of the PLP micelles determined by the pyrene fluorescence method.  
**Figure 7.** Entrapment Efficiencies of PLP polymers and its effects on micelle size. \*p<0.05 compared to free micelles.  
**Figure 8.** Cumulative CycA release from PLP micelles under sink conditions.  
**Figure 9.** Distributions of the logarithms of individual particle diffusion coefficients in water and mucus.

## LIST OF TABLES

### Chapter 4

- Table 1.** PLP polymerization data from <sup>1</sup>H NMR.  
**Table 2.** PLP micelle size.  
**Table 3.** PLP micelle zeta potential and CMC.  
**Table 4.** Diffusion Coefficients (μm<sup>2</sup>/s) and ratio.

## LIST OF ABBREVIATIONS AND SYMBOLS

ATRP	Atom transfer radical polymerization
BRB	Blood retinal barrier
CycA	Cyclosporine A
CMC	Critical micelle concentration
DC	Diffusion coefficient
DLS	Dynamic light scattering
FRP	Free radical polymerization
HPLC	High pressure liquid chromatography
ILM	Inner limiting membrane
IOP	Intraocular pressure
LE	Loteprednol etabonate
MWD	Molecular weight distribution
MWCO	Molecular weight cut off
MPP	Mucopenetrating particles
MPT	Multiple particle tracking
MSD	Mean square displacement
NP	Nanoparticles
NMP	Nitroxide mediated polymerization
OLM	Outer limiting membrane
PBA	Phenylboronic acid
PF127	Pluronic F-127
PAA	Poly(acrylic acid)
PCL	Poly(caprolactone)
PEG	Poly(ethylene glycol)
PEGMA	poly(ethylene glycol) methyl ether methacrylate
PLA	Poly(L-lactide) 2-bromoisobutyryl terminated
PLGA	Poly(lactic-co-glycolic acid)
PPO	Poly(propylene oxide)
PAM	Poly(propylene amide)
PDI	Polydispersity index
PS	Polystyrene
RPE	Retinal pigmented epithelium
RAFT	Reversible addition-fragmentation chain-transfer
STF	Simulated tear film
TEM	Transmission electron micrograph

## CHAPTER 1. INTRODUCTION

The most common method of treating anterior segment diseases of the eye is topical administration in the form of an eye drop. Its low in cost, easy to apply, and non-invasive nature makes it particularly attractive. However, topical medications are quickly removed by precorneal clearance mechanisms and tight barriers of the eye which results in 5% or less of the applied dose reaching intraocular tissues.<sup>4</sup> Precorneal clearance mechanisms such as solution drainage, blinking, rapid tear drainage and turnover, and lacrimal drainage washes away most of the drug within 15-30 seconds. Systemic absorption by the conjunctiva or the nasal mucosa further prevents drug from reaching target tissues.<sup>5</sup> The remaining dose still faces the static and dynamic barriers of the eye including the tight junctions of the conjunctiva, the lipid-water-lipid sandwich of the cornea, tear drainage, and conjunctival blood and lymph clearance.<sup>6</sup> Despite the fact that less than 5% of the topically applied drug permeates the cornea and reaches anterior tissues, topical eye drops remain effective due to the high drug concentrations and frequent administration. This however, can result in side effects such as fatigue, irritation, fainting, dry skin and hyperemia.<sup>7</sup>

A solution is to maintain an effective drug concentration for a sustained period of time through the use of a drug delivery vehicle.<sup>8</sup> Particle delivery systems within the range of 10-1000 nm are referred to as nanoparticles (NPs) and have attracted substantial attention as drug delivery vehicles. The bioavailability, controlled drug release, non-toxic properties, and enhancement of drug solubility associated with these particles makes them particularly attractive. On-going research has been focused on surface functionalization of nanoparticles with ligands to target the ocular mucosa and to increase the precorneal retention time of the drugs.<sup>9</sup> One method is to use mucoadhesive polymers such as chitosan, cellulose, and alginate that interact with the mucin

layer of the tear film through physical entanglements, hydrogen or ionic interactions. Unfortunately, this method is limited by the turnover rate of the mucus and the particles are eventually removed from the precorneal surface.<sup>10</sup> Drugs that are required to be delivered intracellularly must have access to the underlying epithelial cells; for these drugs an attractive alternative method is mucopenetration. Coating NP's with low MW PEG is the most studied penetrating strategy due to its ability to prevent interactions with mucus.<sup>11</sup> This method has been utilized in other mucopenetrating drug delivery systems to vaginal<sup>12</sup>, pulmonary<sup>13</sup>, gastrointestinal<sup>14</sup>, and ocular<sup>15</sup> tissues.

## **1.1 Thesis Objective**

In this thesis, the synthesis of a PEG-based block copolymers to deliver therapeutics to the anterior surface of the eye is discussed. The main focus of this project is to investigate the benefits of mucopenetrating micelles as drug delivery vehicles. Utilizing ATRP will allow for the control of the molecular architecture of the polymer enabling the formation of micelles in water. These modifications can also potentially achieve the second objective of incorporating mucopenetrating properties into the micelles. It is hypothesized that a hydrophilic block, consisting of PEG, will improve the drug bioavailability on the ocular surface. The effect of increasing PEG chain length on physical properties such as size, surface charge, CMC and mucopenetration were studied.

## **1.2 Thesis Outline**

The work in this thesis has been divided into five chapters. The topic and outline of this thesis is included into Chapter 1, as well as an introduction to the research. Chapter 2 is a literature review of the numerous anatomical and physiological barriers of the eye, micelles as

drug delivery systems, and interactions with the tear film. Chapter 3 describes the materials and methods used in this research and Chapter 4 describes the results from the synthesis, characterization, drug release, and mucopenetrative properties of the micelles. Future work and directions of the project will be discussed in Chapter 5 along with conclusions arising from the experiments performed.

## CHAPTER 2. LITERATURE REVIEW

### 2.1 Anatomical and Physiological Barriers

The eyes are organs of the visual system that provide vision; the process of receiving light and translating it into electro-chemical impulses. Rather than being a perfect sphere, the structure of the eye is two-piece unit composed of the anterior segment and posterior segment (Figure 1). The anterior segment of the eye consists of the lens, iris, and cornea. The cornea has a greater curvature than the rest of the eye, and is linked to the larger posterior segment, composed of the vitreous, retina, choroid, and the sclera. The eye can also be divided into 3 layers with each containing various anatomical structures that play a role in the function of the eye. These layers must be bypassed in order to effectively delivery therapeutics to the back of the eye.

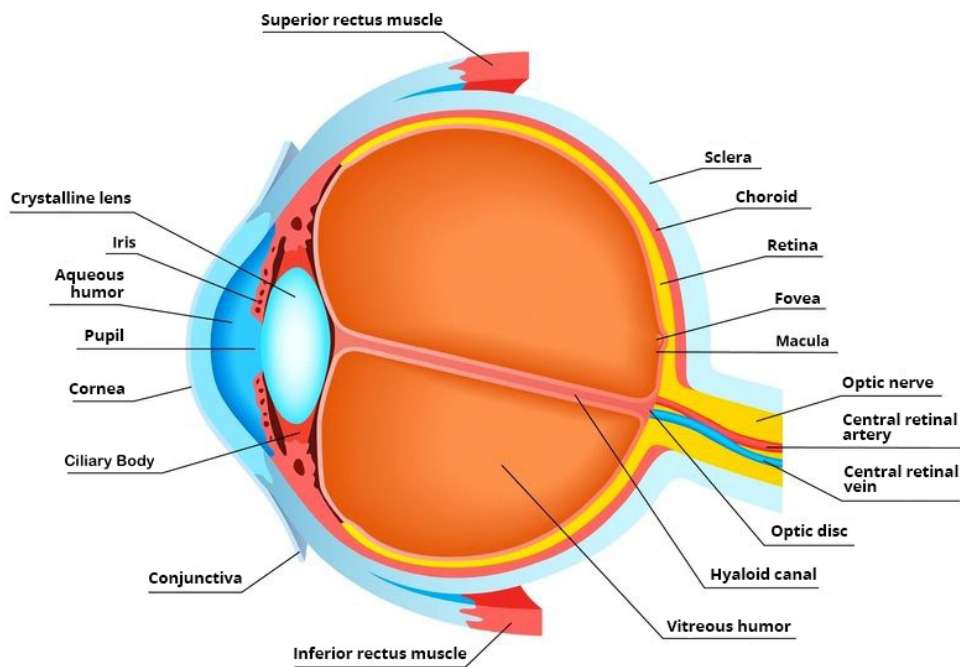


**Figure 1.** Human eye anatomy. Modified from <sup>1</sup>

### 2.1.1 Tear Film

The anterior segment of the eye is coated in a thin layer of tears that lubricate and protect it from debris, pathogens, and irritants. The tear film is composed of an outer lipid layer, middle aqueous layer, and an inner mucin layer. Together, the three layers form the first barrier to the delivery of drugs due to rapid tear drainage and fluid turnover. After the instillation of an eye drop into the eye, the drug mixes with the tear film and therefore, drug residence time becomes a function of lacrimation, tear drainage and turnover, and to some extent the composition of the tear film.<sup>2</sup> The majority of the instilled dose is absorbed systemically by the conjunctiva or the nasal mucosa when rapid tear drainage forces drug through the nasolacrimal duct. The human tear volume is 7  $\mu\text{L}$  and the cul-de-sac can hold up to 30  $\mu\text{L}$  of the administered eye drop.<sup>3</sup> Considering that the average tear turnover time is 2-3 minutes, most of the drug solutions are washed away within 15-30 seconds. As a result, less than 5% of the topically applied drug permeates the cornea and reaches anterior tissues.

The inner mucus layer of the tear film protects the underlying corneal epithelium by trapping pathogens and foreign particulates and therefore represents an additional barrier to ocular drug delivery. The mucus layer is composed of carbohydrates, protein, lipids and inorganic salts. Mucin fibers are large negatively charged glycosylated proteins that form a barrier through electrostatic interactions, van der Waals forces, hydrophobic interactions, hydrogen bonding, and chain entanglement.<sup>4</sup> Laffleur et al. demonstrated that the diffusion rate of neutral poly(acrylic acid) (PAA)-poly(propylene amide) (PAM) nanoparticles (NPs) is 2.5-fold higher than positively charged PAM NP's. Similarly, hydrophobic domains along the mucin strands represent a challenge for hydrophobic drugs and biomaterials such as polystyrene (PS)

and poly(lactic-co-glycolic acid) (PLGA). Therefore, in order to effectively delivery therapeutics to the eye, the tear film must first be overcome.

### **2.1.2 External Fibrous Layer**

The eye can be divided into three concentric layers and the outermost layer is called the fibrous layer, composed of the cornea and the sclera.<sup>5</sup> The cornea is the principle route for topically administered eye drops but it also serves as a major physical barrier to drug adsorption. Intraocular drug bioavailability is low due to tight junctions and the hydrophobic nature of the corneal epithelium. The cornea consists of five layers: the epithelium, Bowman's membrane, the stroma, Descemets membrane, and the endothelium.<sup>6</sup> Bowmans and Descemets membranes are laminar layers that act as basement membranes for the attachment of epithelial and endothelial cells, respectively. They are mainly composed of collagen fibers and do not have significant effect on drug transport. The corneal epithelium is lipoidal in nature and produces a hydrophobic barrier to drug transport. Epithelial cells are joined to one another by desmosomes and surrounded by tight junction complexes which further contribute to the impenetrable surface. Underneath the innermost layer is the stroma that accounts for 90% of the cornea thickness. It is mainly composed of water, mucopolysaccharides, collagen fibers, and a few cells such as keratocytes. The innermost layer of endothelial cells is only a single cell layer in thickness but macula occludens junctions form a tight seal against the aqueous humor. The five layers of the cornea essentially form a lipid-water-lipid sandwich that effectively reduces intraocular drug bioavailability.

The conjunctiva lines the backside of the eyelid and loops back to cover the sclera and the edge of the cornea. It is a thin mucous membrane comprised of columnar epithelial cells that further limit drug delivery with the presence of tight junctions. It also contains goblet cells that

secrete mucin to maintain the tear film. Drug delivery to the conjunctiva is ineffective because a significant amount of drug is lost systemically due to the presence of conjunctival blood capillaries and lymphatics.<sup>5</sup> Alternatively, the sclera is a more effective route of drug delivery but the permeability of the sclera is considered comparable to the corneal stroma. It is composed of an epithelial cell layer and a stroma but is missing an endothelial cell layer. The main functions of the sclera are to act as a barrier to foreign particulates and to maintain the shape of the eye.

The cornea is the classical site of drug entry for topically administered eye drops. Drugs permeate through the cornea by both paracellular and transcellular routes depending on drug size and polarity. Hydrophilic compounds enter mainly through the paracellular route whereas hydrophobic compounds enter transcellularly through the epithelial membrane. However, the lipoidal nature of the corneal epithelium poses a significant barrier for hydrophilic drugs and therefore, the scleral route may be a good alternative. Passage of hydrophilic drugs may be aided by the relatively hydrophilic proteoglycans found within the sclera. Further, sclera permeability is not dependent on drug lipophilicity whereas the cornea is.<sup>3</sup> Small molecules (radius less than 10 Å) can easily permeate through the cornea but large compounds such as macromolecules cannot. Cruysberg et al. determined that human sclera is permeable to compounds up to 150 kDa which allows for the penetration of serum albumins and antibodies. Therefore, the non-corneal route has gained much attention for the delivery of more hydrophilic and large molecules which have poor penetration across the cornea.

### **2.1.3 Middle Vascular Layer**

The middle vascular tunic is usually referred to as the uvea and is composed of the iris, ciliary body, and the choroid.<sup>7</sup> This layer of tissue is primarily responsible for blood flow, ocular

nutrition, and lymphatic drainage but it also presents as a critical barrier. The iris is a pigmented, muscular ring that controls the amount of light entering into a central aperture called the pupil. It is often a target of drug delivery for regulating pupil size but for other target tissues, the iris has considerable effects. Due to heavy pigmentation, the iris can act as a drug reservoir for lipophilic substances that absorb to pigment granules. This effect can substantially decrease the initial dose, but it can also improve drug release kinetics by allowing long-term storage and slow release through low affinity and nonspecific binding.

The ciliary body is a heavily muscled ring of tissue with an extensive capillary bed that is responsible for lens attachment and shape. The inner layer faces the vitreous body and is nonpigmented until it reaches the iris, whereas the outer layer contains numerous pigment granules and continues posteriorly with the retinal pigment epithelium (RPE). Since there are no tight junctions in the capillary network, drug diffusion in and out of the ciliary body can be significant. This is a good route of entrance into the aqueous humor but there are however, tight junctions between the inner and outer layers of the ciliary body and this forms a barrier to the posterior chamber of the eye. Similar to the iris, pigment granules in the outer layer absorb and store drug but they also assist in the detoxification of drugs because there are extensive metabolic enzymes in the ciliary body. Enzymes such as P450 were demonstrated by Asakura et al. to have highest activity in the ciliary body compared to different ocular tissues, specifically in the non-pigmented epithelial cells.<sup>8</sup> Other enzymes such as ketoreductases, aldehyde reductase, histamine-N-methyltransferase and glutathione-S-transferases were also found in the ciliary body by Argikar et al.<sup>9</sup> The presence of these metabolic enzymes detoxify many classes of drugs before reaching the target tissues and the pigment granules further assist metabolism and removal by storing and slowly releasing the drug.

The choroid is a highly vascularized connective tissue with large lymphatic channels. It is loosely attached to the sclera with an area, the suprachoroidal space, that can be instilled for intraocular delivery. The suprachoroidal space is gaining much attention because it targets the choroid, RPE, and retina with high bioavailability.<sup>10</sup> However, the inner choriocapillaris that allow for the quick exchange of nutrients can also uptake drug and cause it to enter systemic circulation. Choroidal circulation accounts for 85% of the total blood flow in the eye and this high-flow system can significantly reduce drug concentrations in the eye.<sup>11</sup> Further, between the choriocapillaris and retina is the Bruchs membrane that can act as a partial barrier between tissues and even if a drug successfully penetrates it, the inner neural layer and blood retinal barrier still poses a challenge.

#### **2.1.4 Internal Nervous Layer**

The retina is the most important tissue of the eye which converts light into neural signals, upon which visual images are perceived in the brain. Treatment for ocular diseases such as glaucoma, diabetic retinopathy, and age-related macular degeneration require high drug concentrations to target retinal cells but this remains to be the biggest challenge of ocular delivery.

Functionally, the retina can be divided into two areas. The outer retina consists of the photoreceptor neurons and the inner retina consists of all other retinal neurons. Müller cells that are present in the retina span the width and form a tight barrier against the vitreous body. Known as the inner limiting membrane (ILM), it is not a true membrane but rather fused foot processes of the Müller cells that seal the neural retinal from the vitreal body. This is also true for the outer surface of the retina in which tight junctions between Müller cells and photoreceptor cells form the outer limiting membrane (OLM). Along with these barrier functions, Müller cells also

participate in the establishment of the blood-retinal-barrier (BRB) by expressing factors that induce the tight junctions between endothelial cells.<sup>12</sup> Therefore, Müller cells are very important in maintaining the barrier function of the retinal vasculature but unfortunately, this also prevents the passage of therapeutic drugs.

The BRB protects the eyes from fluctuations in blood constituents, toxins and other foreign compounds including many drugs. Large molecules and substances that can potentially harm the retina are filtered out before entering the vitreous and aqueous humor. The BRB consists of two parts: the retinal vasculature and the RPE. In the retina, the endothelial cells are different from peripheral tissues in that they contain belt-like zonula tight junctions. These junctions that are only present in the brain and the retina prevent paracellular transport of water-soluble substances and only through transcellular transport can molecules enter. Although the RPE is not formally part of the inner neural layer since it is not intrinsically part of the neural retina, photoreceptor cells will die without proper RPE function. The RPE cells play a huge role in controlling fluid, nutrient, and waste removal from photoreceptors. It consists of a monolayer of pigmented neuroepithelial cells that are laced together by tight junctions. Similar to the endothelial cells of the retinal vasculature, they contain belt-like zonula tight junctions that stop paracellular movement of substances from the permissive choroid. The RPE also has a metabolic function and the presence of these enzymes can detoxify drugs. Pigment granules further assist in this process by storing and slowly releasing the drug for metabolism. Together, tight junctions, pigment granules, and metabolic enzymes form a nearly impenetrable surface that prevents the passive diffusion of substances into the retina.

## 2.2 Ophthalmic Drug Delivery Methods

Maintaining an effective drug concentration in the therapeutic window remains to be a challenging task. Numerous barriers and rapid clearance prior to reaching underlying tissues significantly reduce drug concentration. Many of these drug systems require frequent administration at high doses to compensate for drug loss and systemic exposure. The effect is a cycle of under and overexposure of drug often at toxic levels (Figure 2). An ideal system would be able to provide a constant therapeutic dose for a period of time. This requires the system to escape the barrier mechanisms of the eye. Some of the current traditional ophthalmic drug delivery systems are discussed below (Figure 3).

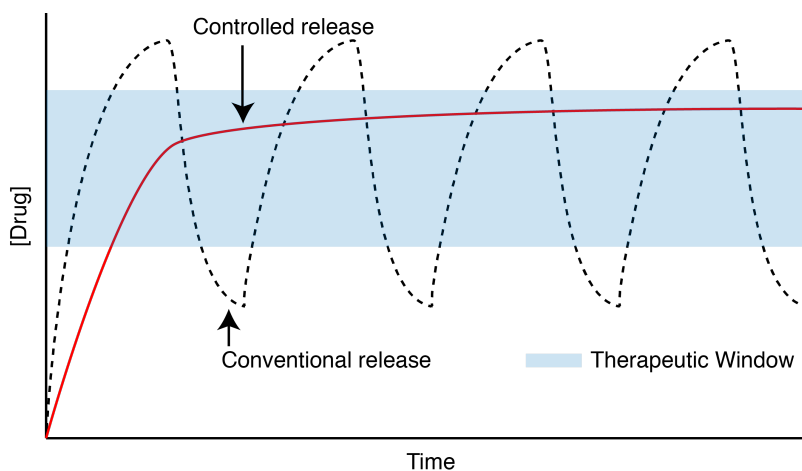


**Figure 2.** Conventional vs. Controlled drug release.

### 2.2.1 Topical Administration

Topical administration in the form of eye drops is the most common method of treating anterior segment diseases. However, precorneal clearance mechanisms such as solution drainage, blinking, rapid tear drainage and turnover, and lacrimal drainage results in only 5% of the applied dose reaching intraocular tissues.<sup>3</sup> Upon the instillation of an eye drop (25-50  $\mu\text{L}$ ) the volume exceeds the capacity of the conjunctival sac (10 mL) and consequently, majority of the solution drains out of the eye or moves to the nasolacrimal duct for systemic absorption. Infants

and young children are especially subject to much higher risks because drug adsorption and corneal permeation is more rapid due to immature barriers.<sup>13</sup> Palmer et al. found that the blood levels of timolol in children ranged from 3.5-34 ng/mL in comparison to adults that were no more than 2.45 ng/mL.<sup>14</sup> This resulted in side effects such as fatigue, irritation, fainting, dry skin, hyperemia, and more serious behavioural changes such as delirium. From the initial instilled dose, the concentration of drug in the anterior chamber is reduced two orders of magnitude and is still susceptible to elimination. Aqueous turnover through the chamber angle and Schlemm's canal eliminates drug at a rate of 3  $\mu\text{L}/\text{min}$ . Lipophilic drugs are cleared at a higher rate of 20-30  $\mu\text{L}/\text{min}$  due to their ability to penetrate the endothelial walls of uveal blood vessels. The net effect is a short half-life of approximately an hour in the anterior chamber and the inability of reaching posterior segment targets. Despite the fact that less than 5% of the topically applied drug permeates the cornea and reaches anterior tissues, topical eye drops remain effective due to the high drug concentrations and frequent administration.

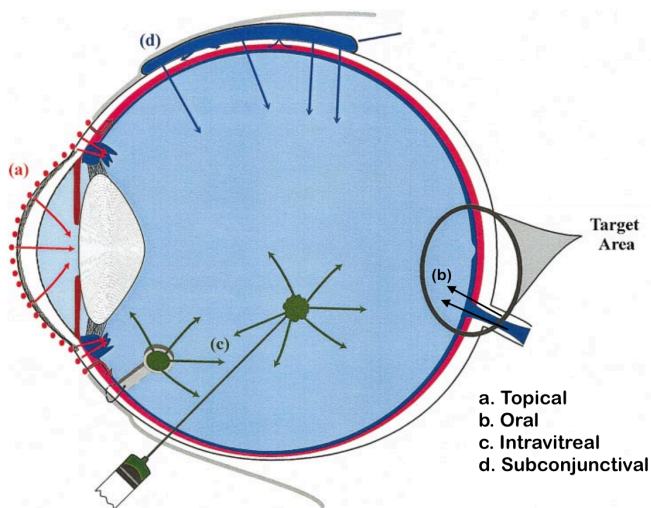


**Figure 3.** Routes of drug administration to the eye. Adapted from <sup>2</sup>

### **2.2.2 Oral Administration**

Oral administration of drugs has been studied as a possible non-invasive route to treat retinal diseases. As previously mentioned, molecules in the systemic circulation must cross the blood-aqueous and blood-retinal barrier in order to enter the ocular tissues.<sup>3</sup> An additional barrier to oral administration is digestion and drug metabolism in the liver before the drug even reaches the systemic circulation. It is a very infrequent method of ophthalmic drug delivery because it requires high dosage in order to observe any significant effect. For example, oral carbonic anhydrase inhibitors such as acetazolamide were once used for glaucoma treatment but have been discontinued due to high systemic toxicity and side effects.<sup>15</sup> As a result, oral administration for the treatment of ocular diseases is rarely encountered.

### **2.2.3 Subconjunctival Injections**

Subconjunctival administration involves the injection of drug solutions into the subconjunctival space to form a localized depot, which may allow for long-term sustained drug delivery to posterior tissues. The subconjunctival space is located behind the conjunctiva and outside of the sclera. This method of administration is less invasive than intravitreal injections and bypasses the conjunctival epithelium, precorneal clearance and corneal barriers to have direct access to the transscleral route.<sup>16</sup> After subconjunctival injection, drugs must penetrate the sclera, which is more permeable than the cornea and thus, feasible to the delivery of drugs to the choroid. However, as previously discussed, the choroidal vasculature presents a significant barrier as high choroidal blood flow can eliminate a significant fraction of drug before it reaches the RPE. Furthermore, the RPE and BRB limits drug bioavailability in retinal tissues. Compared to topical administration, subconjunctival administration significantly increases drug concentrations to the uvea and overcomes the inability of reaching the neural retina. Despite all

these facts, drug elimination into conjunctival lymphatics before sclera penetration is a major determinant of vitreous drug levels. Therefore, longer residence times on the scleral surface through the incorporation of a biomaterial can improve subconjunctival delivery.

#### **2.2.4 Intravitreal Injections**

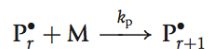
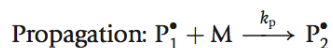
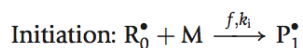
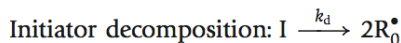
Direct drug administration into the vitreous offers the advantage of straightforward access to the vitreous and retina. It is the most efficient mode of drug delivery to the posterior segment but numerous barriers still exist. Drug elimination can occur through anterior and posterior routes depending on the size, polarity, and charge of the drug.<sup>17</sup> The anterior route of drug elimination through aqueous turnover and uveal blood flow is accessible to all compounds, whereas the posterior route is limited to small lipophilic compounds that can permeate the BRB. As a result, the half-life of small molecules (<500 Da) is <3 days and these compounds require frequent injections.<sup>18</sup> One method of achieving longer retention times is with larger compounds or tethering of drugs to polymers but their effect on the retina may be limited due to the ILM cut off of >40 kDa. The advantages of IVIs are their ability to achieve high concentrations of drug in the posterior segment with minimal systemic toxicity but its invasive nature is associated with many complications. The list includes intraocular pressure (IOP) increase, intraocular bleeding, retinal detachment, endophthalmitis, and cataracts.<sup>19</sup> Smith et al. determined that there is a positive correlation between the rate of retinal detachment and number of retinal breaks. One solution is to create an adhesion surrounding retinal breaks with laser photocoagulation or cryotherapy but ultimately, the underlying problem is with the injection itself.<sup>20</sup> Therefore, it is important to design formulations to maintain the therapeutic drug concentration over prolonged periods to minimize the number of injections. Nanoparticles, micelles, liposomes, and thermoresponsive polymers may be incorporated to increase the half-life of a drug.

The difficulty in getting drug penetration within the eye and movement to target sites remain a challenging task. Numerous physiological, anatomical, and metabolic barriers result in drug clearance and ineffective drug delivery to ocular tissues. The aim of this research is to increase the bioavailability of topically administered drugs to reduce dosage, frequency, side effects, and toxicity. The current work is focused on the development of a drug delivery vehicle with controlled, sustained release of Cyclosporine A (CycA) to the anterior segment of the eye.

## 2.3 Polymerization Techniques

### 2.3.1 Free Radical Polymerization

Conventional free radical polymerization (FRP) is the most commonly used method due to its versatility to a wide range of monomers, its low cost and ease in terms of conditions, operations, and performance.<sup>21</sup> FRP can be described by three primary reactions shown in Figure 4. They are initiation, propagation and termination.



Termination (note:  $k_t = k_{td} + k_{tc}$ ):

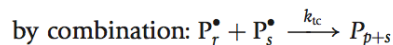
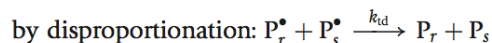


**Figure 4.** Mechanism of Free Radical Polymerization. Adapted from <sup>22</sup>

In a typical FRP reaction, the first step is the hemolytic cleavage of initiator through chemical, thermal, or radiation stimulation (Figure 4).<sup>22</sup> The production of a radical species initiates propagation by reacting with alkene bonds and forming the polymer backbone. Free radicals can terminate by either combination or disproportionation. Termination through

combination is the result of two radicals coming together and forming a stable bond, whereas disproportionation is the abstraction of a hydrogen atom from one of the end chains to form two dead polymer chains. Termination in FRP is diffusion limited and as a result, the molecular weight distribution (MWD) and polydispersity index (PDI) are broad. Solution and suspension methods can improve the heat transfer and viscosity but the lack of MW control produces batch to batch variability. This can be a huge problem when developing polymeric systems with tunable properties which rely heavily on polymer composition.

### **2.3.2 Controlled/Living Polymerization: Atom Transfer Radical Polymerization**

FRP lacks the ability to control molecular weights, narrow dispersity and molecular architecture. Controlling molecular architecture in FRP was considered impossible because two radicals always terminate at a very fast, diffusion controlled rate. In fact, living polymerization is the only viable technique for producing polymers with controlled molecular structures.<sup>23</sup> The mechanism of living polymerization and conventional FRP are fairly similar since they follow the same 3 steps: initiation, propagation, termination. What's different in living polymerization is that it undergoes an additional activation/deactivation process that prolongs the life of propagating radicals. For each millisecond of activity there exists dormant periods of 1 minute and hundreds of dormancy periods extend the life of propagating chains from 1 second in FRP to more than a day in living radical polymerization. The advantages of this process will be further discussed below.

Atom transfer radical polymerization (ATRP) is used to synthesize polymers with precisely controlled molecular weights and relatively low polydispersities. Since its discovery in 1995, it has gained considerable attention from the industry and academia for its ability to produce polymers with controlled architecture.<sup>24</sup> The ATRP mechanism is a catalytic process

that involves an alkyl halide initiator, ligated metal salt, and monomer (Figure 5). A radical species ( $R^*$ ) is formed from a reversible reaction between the alkyl halide initiator ( $RX$ ) and ligated metal salt ( $Mt^nY/Ligand$ ), which can undergo subsequent propagation reactions with monomer units.<sup>25</sup> It can also be deactivated with the oxidized catalyst ( $Mt^{n+1}Y/Ligand$ ) to form dormant polymer chains ( $R_n-X$ ) and the reduced form of the catalyst ( $Mt^nY/Ligand$ ). This equilibrium between propagating radicals and dormant species is attributed to the long life time of propagating chains where termination is strongly suppressed. ATRP polymerization can be used to synthesize a variety of polymers with complex macromolecular architecture. This includes branched structures formed by copolymerization of macromonomers, grafting onto and from functional backbones, and copolymers formed using multifunctional initiators. These structures can be used to alter biomaterial and NP properties to improve drug delivery systems.

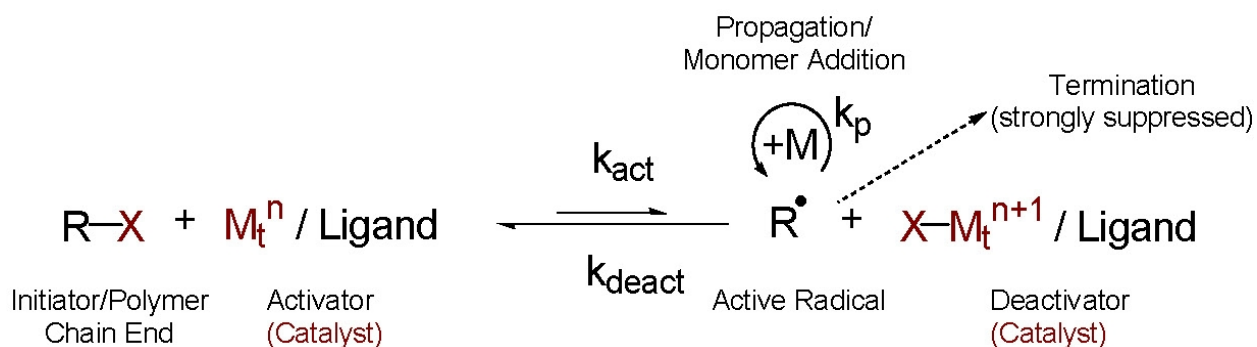


**Figure 5.** ATRP polymerization mechanism. Adapted from <sup>23</sup>

Other types of living polymerization techniques include reversible addition-fragmentation chain-transfer (RAFT) and nitroxide mediated polymerization (NMP). All three techniques can effectively control the macromolecular architecture but differ in versatility and robustness. ATRP and RAFT can be utilized in wide range of temperatures while NMP is limited to high temperatures above 100 °C.<sup>26, 27</sup> NMP is also limited to the polymerization of styrene's and lack the range of monomer applicability that is seen in ATRP and RAFT. A major advantage of

ATRP is the fact that it is a catalytic process and tiny amounts of catalyst are sufficient for the growth of many polymeric chains. In contrast, other methods require an equal-molar concentration of either chain transfer agent for RAFT or nitroxide for NMP for every growing polymeric chain, which can become tedious during purification. This is very beneficial from a cost perspective and gives ATRP the most commercial potential compared to the other methods. Therefore, ATRP was chosen as the polymerization technique because it can be applied to a wide range of monomers, temperatures, processes, and is more tolerant to water and oxygen impurities.

## **2.4 Polymeric Micelles**

Over the recent years, NP's have increasingly been used in ocular delivery because of their stability, efficient drug loading, prolonged retention and circulation time. To date, various polymer-based nanocarriers such as NP's, dendrimers, and liposomes have been exploited as drug delivery vehicles. However, the majority of these formulations are administered through intravitreal or subconjunctival injections which is associated with adverse effects. Growing evidence suggests that polymeric micelles as nanocarriers have the potential to overcome such limitations and provide therapeutic drug concentrations at anterior and posterior tissues.

### **2.4.1 Micelle Formation and Critical Micelle Concentration**

Nanosized micelles, also called nanomicelles, consist of a hydrophobic core and a hydrophilic shell.<sup>28</sup> These polymeric micelles are based on amphiphilic molecules or block copolymers that can self-assemble into organized core-shell structures. Such a process is favoured thermodynamically where the hydrophilic chains cover the hydrophobic core to avoid contact with water and therefore, reducing the interfacial free energy of the polymer-water system. The critical micelle concentration (CMC) is the minimal polymer concentration required

to form micelles. Below the CMC, polymer chains are uniformly distributed in solution until there is a sufficient amount to form an aggregate, which is known as the CMC. Polymeric micelles typically have CMC values ranging from  $10^{-6}$ - $10^{-7}$  M with decreasing values indicative of increased stability. This is a crucial factor for topical micellar formulations because it determines the chances of premature drug release.<sup>29</sup> Another important factor that influences micelle stability is the PDI. The dispersity of the polymer influences its kinetics between the micellar and non-micellar state and so having low dispersity's of <1.2 are preferred. Depending on the polymer composition, micelles can take up different shapes including spherical, cylindrical and star shaped structures.

The ability of polymeric micelles to solubilize and stabilize hydrophobic drugs improves therapeutic outcomes. Nevertheless, micelles still suffer from protective properties of the eye. Dilution in the tear film as well as interactions with the components lead to their premature elimination.

#### **2.4.2 Ocular Delivery Pathways of Micelles**

After the topical administration of an eye drop, the drug formulation is anticipated to follow either the corneal or conjunctival-scleral pathway to reach the tissues of the anterior and posterior segment. The rate limiting barrier for hydrophobic drugs is the hydrophilic stroma that makes up 85-90% of the cornea. These limitations can be overcome by encapsulating hydrophobic drugs into the lipophilic core of polymeric micelles. Polymeric micelles can penetrate the cornea and conjunctival scleral pathway owing to their small nature. The high permeability of the conjunctiva compared to the cornea is attributed to the larger surface area (17 fold) and paracellular spacing in conjunctival tissues (>230x). However, this is not the preferred route because lymphatics and blood vessels eliminate a significant amount of drug into systemic

circulation. Alternatively, the scleral pathway minimizes drug removal by systemic circulation and is more penetrable than the cornea. For this reason, the scleral route may be preferred over the corneal pathway. Regardless of the pathway, once it has reached posterior tissues it may be engulfed by RPE cells by endocytosis to generate therapeutic concentrations in the neural retina.

### **2.4.3 Micelle Structure**

Polymeric micelles can be divided into three categories: 1. Polymer-drug conjugates 2. Drug encapsulated micelles 3. Polyion complex micelles.

#### **1. Polymer-drug conjugates**

These are developed through hydrolysable chemical bonds between the functional groups of the polymeric backbone and the drug. The numerous functional groups on polymer backbones can enable a variety of chemical reactions for drug conjugation. Poly(ethylene oxide)-*b*-poly(ester) and poly(ethylene oxide)-*b*-poly(amino acid) block copolymer based conjugates have been extensively studied for drug delivery applications.<sup>29</sup>

#### **2. Drug encapsulated carriers**

Solubilization and encapsulation of drug into the polymeric core can be accomplished by either chemical or physical methods. Chemical methods involve covalent core cross-linking of the polymer with drug. Similar to polymer-drug conjugates, different functional groups on the polymer can be reacted with the drug. Commonly used methods include FRP, addition of bifunctional crosslinker, and disulphide bridges.<sup>30</sup> Chemical cross linking improves circulation kinetics, prevents premature release, and increases target site drug bioavailability but the chemical reactions may sometimes be challenging and complicated. Therefore, physical methods are simpler and more practical. They include direct dissolution, dialysis, oil-in-water emulsion, solvent evaporation, co-solvent

evaporation and freeze drying methods. The direct dissolution method is the simplest technique and it will be discussed in Chapter 3 to prepare drug-loaded polymeric micelles.

### 3. Polyion complex micelles.<sup>31</sup>

Electrostatic interactions between oppositely charged polymer and drug results in polyion complex micelles. This method is suitable for therapeutics that carry charge such as DNA and peptides. Harada-Shiba et al. prepared polyion complex micelles with poly(L)lysine-*b*-poly(ethylene glycol) block copolymer to improve the intravenous delivery of DNA.<sup>32</sup> These *in vivo* studies showed a significant increase of gene expression for 3 days.

#### **2.4.4 Drug Release from Polymeric Micelles**

Drug release from polymeric micelles depends on the method used for their preparation, the structure of the micelle, the physicochemical properties, and the localization of drug in the polymeric micelles.<sup>30</sup> In general, drug release from polymer-drug conjugates follows two mechanisms (Figure 6).

1. Dissociation of micelles followed by drug cleavage from the polymeric unimers
2. Drug cleavage inside the micelle core followed by diffusion out of the particle

In contrast, drug release from polyion complex micelles is triggered by ion exchange and release from drug-loaded micelles proceeds by diffusion. Micelle-forming drug conjugates are expected to have the slowest drug release followed by drug encapsulated and polyion complex micelles. Yoo et al. chemically conjugated Doxorubicin to poly(ethylene oxide)-*b*-poly(D,L-lactic-co-glycolic acid) to improve the sustained release of drug.<sup>33</sup> These studies showed that drug-conjugated micelles improved drug release from 3 days to 2 weeks.

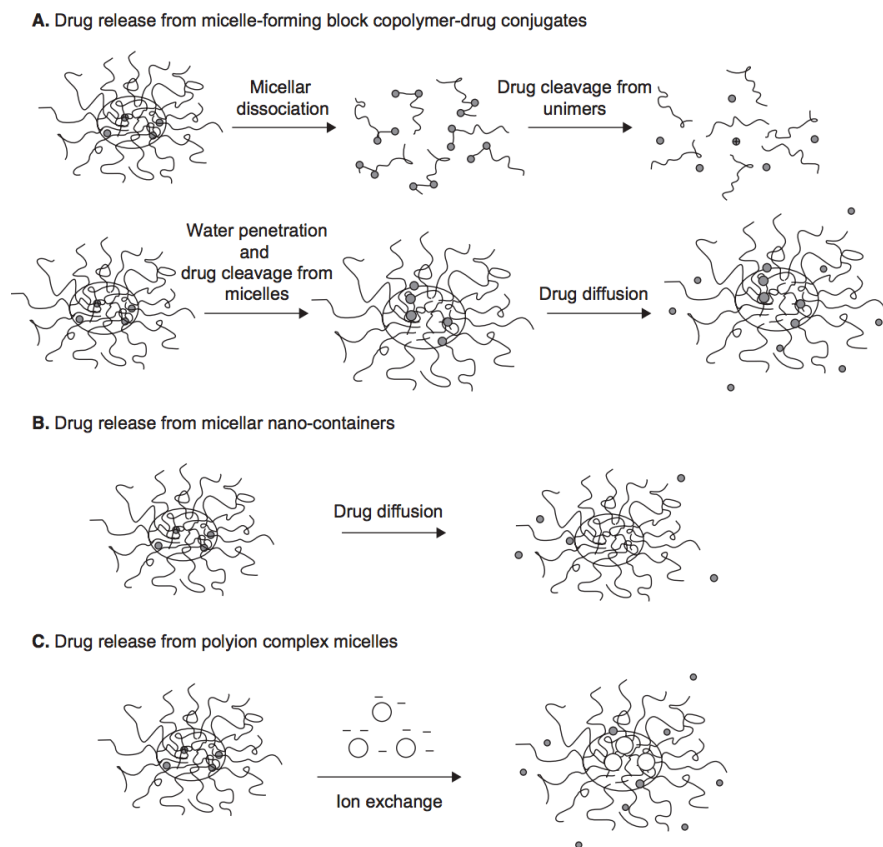


**Figure 6.** Drug release mechanisms from polymeric micelles. Adapted from <sup>29</sup>

In addition to these two release mechanisms, different types of release profiles including instant, sustained, pulsed or delayed drug release can be achieved by tailoring the chemical structure of the block copolymers.<sup>29</sup> For example, increasing the hydrophobicity and rigidity of the micellar core can restrict the penetration of water and free ions in micelle-forming drug conjugates to sustain or even delay drug release. The opposite effect can be accomplished by incorporating cleavable linkers or more sensitive chemical bonds to induce a faster or instant drug release. The ability to fine tune the drug release of micelles for a particular application makes them excellent candidates.

## 2.5 Interactions with the Mucus Layer

One of the greatest challenges that limits the success of NP's is their ability to penetrate quickly through ocular mucin to reach underlying tissues. Mucus is a viscoelastic and adhesive hydrogel that is composed primarily of crosslinked mucin fibers secreted by conjunctival goblet cells. It protects the underlying epithelium from the external environment by trapping pathogens and foreign particulates. Unfortunately, NP's and other therapeutics are also trapped and rapidly removed by mucus. Mucus forms interactions with particulates through electrostatic, van der Waals forces, hydrophobic forces, hydrogen bonding, and chain entanglement.<sup>34</sup> These interactions are maximized in mucoadhesive particles to prolong the retention time of the particle on the mucosal surface. Alternatively, a nanocarrier that can effectively penetrate the mucus layer can also achieve longer retention times on the cell surface. These two mechanisms are depicted in Figure 7 and are methods of increasing ocular drug bioavailability.<sup>35</sup>

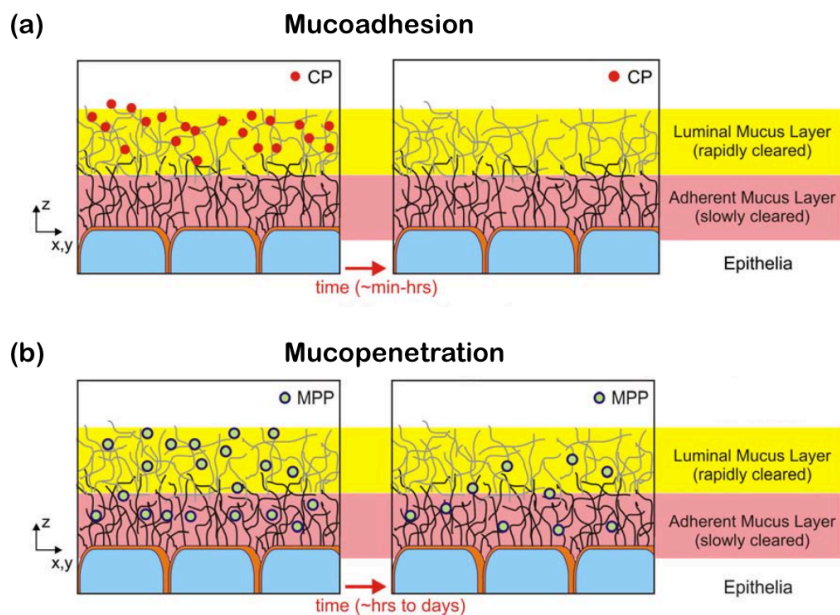


**Figure 7.** The fate of (a) mucoadhesive and (b) mucopenetrating particles in mucus. Modified from<sup>35</sup>.

### 2.5.1 Mucoadhesion

One of the biggest problems with conventional eye drops is that most of the drug solution is washed away within minutes. Only 5% of the administered dose reaches the anterior tissues because the drug residence time is a function of lacrimation, tear drainage and turnover. One method of increasing drug residence time and subsequently, the drug bioavailability, is to use mucoadhesive polymers. There are numerous classes of mucoadhesive polymers but the focus of this thesis will be anionic, cationic, polymeric thiomers, and boronic acid copolymers.<sup>36</sup> Anionic polymers such as PAA, alginate and cellulose derivatives, and pectin have mucoadhesive properties based on physical entanglements, hydrogen or ionic interactions. These polymers were found to be strongly mucoadhesive in acidic conditions when in the protonated state, suggesting an increase in hydrogen bonding between carboxylic acid residues and mucins.<sup>37</sup> The positive correlation between acrylic acid composition in the copolymer and the mucoadhesive performance further confirms the role of carboxylic acid groups in bonding. Cationic polymers such as chitosan and some polymethacrylates have been reported as excellent mucoadhesive polymers. Electrostatic interactions with the negatively charged mucin is the major mechanism but further reinforcement with hydrogen bonding and hydrophobic effects enhances mucoadhesive properties. In both anionic and cationic polymers, thiolation is a method of increasing mucoadhesion by forming disulfide bonds between sulfhydryl groups of the polymer and cysteine domains of mucus. Some examples of polymeric thiomers include PAA/cysteine, chitosan/thioglycolic acid, alginate/cysteine, and thiolated hydroxyethyl cellulose.<sup>36, 38</sup> A more recently discovered class of mucoadhesives is boronic acid copolymers. The mucoadhesive properties of boronic acid have been related to its ability to interact with 1,2-cis-diols of sialic acid residues on mucin.<sup>39</sup> Its complexation with mucins is most pronounced in neutral and

weakly basic pHs of 7-9 making it very applicable in the eye. Previously in the Sheardown group, phenylboronic acid (PBA) was incorporated into polymer micelles to improve topical drug delivery of CycA.<sup>40</sup> The micelles showed low cytotoxicity, good biocompatibility and excellent mucoadhesion *in vitro*. Mucoadhesive properties offer promising results and the potential to improve drug bioavailability but this approach is limited by the turnover rate of the mucus layer. Although the turnover rate of the mucus layer is much slower than of the tear film, the mucins are eventually removed from the precorneal surface.<sup>41</sup> For drugs that are required to be delivered intracellularly they must have access to the underlying epithelial cells and so an alternative to mucoadhesion is mucopenetration.

### **2.5.2 Mucopenetration**

To overcome the shortcomings of mucoadhesion and still provide longer residence times for particles at mucosal surfaces, it is desirable to engineer particles that can effectively cross the mucus barrier. Also known as mucopenetration, the composition and properties of mucus highlights three factors that governs mucopenetrative properties: size, charge and hydrophobicity. Nanocarriers must be small enough to avoid steric obstruction and have a near neutral surface to prevent the formation of electrostatic interactions with negatively charged mucins. They also must be hydrophilic to evade the numerous hydrophobic regions along mucin strands. These three factors must be incorporated when designing the mucopenetrating particles (MPP).

Modification of surface physiochemical properties is the main method of achieving mucopenetrative properties. Polyethylene glycol (PEG) is a neutral hydrophilic polymer that is used widely in pharmaceuticals to decrease protein adsorption and improve systemic circulation. Coating NPs with low molecular weight PEG is the most studied penetrating strategy although

the exact mechanism is not understood. Mucopenetration was first demonstrated by Hanes et al. where he studied diffusion rates of PS NPs coated with different PEG MWs and densities.<sup>35</sup> It was determined that low MW (2 kDa) and high density (65-70%) PEG coatings facilitate passage through the mucus. It is hypothesized that 1. low MW PEG chains are unable to support adhesion through interpenetration and 2. high PEG density generates a hydrated cloud with large volume that prevents interactions with hydrophobic components. Mucopenetrating properties can also be achieved in micelles with a PEG corona. Taipaleenmäki et al. synthesized mucopenetrating micelles using block copolymers of linear PEG-poly(caprolactone) (PCL) to cross the intestinal mucus layer.<sup>42</sup> The micelles were able to diffuse through a mucus layer produced by epithelial cells to deliver a model drug. Another polymer that exhibits mucopenetrative properties is Pluronic F-127 (PF127). PF127 is a triblock copolymer of PEG-poly(propylene oxide) (PPO)-PEG and has numerous applications in oral, intravenous and ophthalmic administration. Adsorption of the hydrophobic PPO segment to a particle surface leaves PEG segments protruding out in a similar fashion to covalent conjugation of PEG to NP surfaces. Studies with coated and uncoated PLGA particles indicate that PF127 significantly improves the speed of particles in mucus up to 900x. More recently, Schopf et al. prepared loteprednol etabonate (LE) MPPs by wet nanomilling with F127 to deliver drugs to the eye.<sup>43</sup> In a rabbit vascular leakage model, these particles were shown to deliver effective drug concentrations of LE to the back of the eye, which suggests that topical administration can reach posterior segment targets. Unfortunately, there have only been a few studies reporting the production of particles with sizes <100 nm through wet media milling.<sup>44</sup> These LE MPPs had an average hydrodynamic diameter of 240 nm and at this size, they likely became immobilized by the small pores of the mucus mesh. Therefore, it would be superior to develop a nanocarrier <100 nm with mucopenetrating

properties. The small sizes of polymeric micelles (<100nm) is expected to migrate deeper into the mucosal layer to provide higher drug concentrations at target tissues.

## 2.6 Diffusion Systems

Different diffusion systems have been developed to evaluate the interactions between NPs and micelles such as side-on-three compartment diffusion and multiple particle tracking (MPT).<sup>45</sup> Side-on-three compartment is the most commonly used method and consists of membrane-separated donor, acceptor, and central compartments. The particles and the mucus model is placed in the donor and central compartment, respectively, and the arrival of the particles in the acceptor compartment is evaluated over time. However, the membranes used to separate the compartments have the capacity to retain particles and so the effects of the membrane vs the mucus must be distinguished. An alternative method is to analyze the trajectories of fluorescent particles in mucus bulk by MPT. This method avoids the effects of membranes on diffusion as only one compartment is required. The motion of hundreds of fluorescent particles is recorded by video microscopy and analyzed to determine the diffusion coefficients.

### 2.6.1 Multiple Particle Tracking and Mean Square Displacement

The mobility of the particle can be described by the mean-square displacement (MSD). MSD is defined as<sup>46</sup>:

$$MSD = \langle \Delta r(\tau)^2 \rangle = \langle [r(t + \tau) - r(t)]^2 \rangle$$

where  $r(t)$  is the position of the particle at time  $t$  and  $\tau$  is the lag time between two positions taken by the particle and used to calculate the displacement. The MSD reflects the mechanical properties of the environment and can be obtained by MPT. Individual trajectories of the particles obtained by video microscopy can be analyzed to determine MSD values over different

time scales. Subdiffusive transport in 2D, the MSD is related to the medium in which the particles are moving through the equation:

$$MSD = 4D\tau^\alpha$$

The diffusion coefficient (DC) can be subsequently calculated by fitting the MSD vs  $\tau$  to a linear function.

$$\log(MSD) = \alpha \log \tau + \log(4D)$$

The log-log plot illustrates that the MSD varies linearly with the lag time,  $msd(\tau) \propto \tau$ .<sup>47</sup> This is a characteristic of the Brownian motion observed in a purely viscous (or Newtonian) fluids such as water.  $\alpha$  represents the slope of the curve which is equal or close to one for a particle moving in Brownian motion. In simple diffusion, the DC is independent of  $\tau$  and thus,  $\alpha$  is equivalent or close to 1. The Stokes-Einstein relation,

$$D = \frac{k_B T}{6\pi\eta r}$$

(where  $k_B$  is Boltzmann's constant,  $T$  is temperature in Kelvin,  $\eta$  is fluid viscosity and  $r$  is the particle radius) can be applied to particles transporting in simple diffusion to determine the size of the particle and viscosity of the medium. This method has been used extensively in the literature for the investigation of mucopentrating properties. Similarly, we will be applying this method to our micelles in ocular mucus.

## CHAPTER 3. MATERIALS AND METHODS

### 3.1 Materials

All solvents and reagents were purchased from Sigma Aldrich (Oakville, ON, Canada) and used as received unless otherwise noted. Acetonitrile, methanol, toluene, tetrahydrofuran, anhydrous diethyl ether, and anhydrous ethanol were purchased from Caledon Laboratories (Caledon, ON) and used as received. Cu(I)Br  $\geq 97\%$  was purchased from Sigma-Aldrich, stirred in glacial acetic acid overnight, rinsed with ethanol and diethyl ether, and stored under nitrogen to prevent oxidation. Poly(L-lactide), 2-bromoisobutyryl terminated (Sigma Aldrich, Milwaukee, WI) was used as received in the synthesis of pLA-*b*-pEGMA. Linear pLA-PEG was purchased from PolySciTech (West Lafayette, IN). Purified water with a resistivity of 18.2 M $\Omega$  cm was prepared using a Milli-pore Barnstead water purification system (Graham, NC, USA). Cellulose dialysis membranes with molecular weight cut-off (MWCO) values of 3.5 and 14 kDa were purchased from Spectrum Laboratories Inc. (Rancho Dominguez, CA, USA). Acrodisc CR 13 mm high pressure liquid chromatography (HPLC) grade syringe filter with a 0.2  $\mu$ m pore size were purchased from PALL Life Sciences.

### 3.2 Synthesis of pLA-*b*-pEGMA

pLA-*b*-pEGMA copolymers were synthesized by ATRP polymerization. In a typical reaction procedure, (30:1:1:2 molar feed ratio of pEGMA:pLA:CuBr,Bpy), poly(ethylene glycol) methyl ether methacrylate (pEGMA, 500 Da, 749 mg, 1.5 mmol) and poly(L-lactide) 2-bromoisobutyryl terminated (pLA, 10 kDa, 275 mg, 0.05 mmol) were dissolved in 7.0 mL of 71:29 dimethylsulfoxide:acetonitrile and the mixture was purged with nitrogen. In a separate schlenk tube containing a stir bar, CuBr (7.16 mg, 0.05 mmol), and 2,2'-Bipyridyl (Bpy, 16 mg, 0.1 mmol), oxygen was removed followed by backfilling with nitrogen. This process was

repeated 3 times to ensure the removal of oxygen and was followed by the addition of the pLA:pEGMA solution. The flask was then heated to 80 °C and the reaction was allowed to proceed for 24 hours under constant stirring. After the solution was allowed to cool to room temperature, it was filtered through a silica column to remove CuBr. The filtrate was then concentrated by rotary evaporation, resuspended in purified water and then dialyzed for 4 days, with water changes occurring daily. The solution was concentrated by rotary evaporation and the copolymer was isolated by precipitation into cold anhydrous diethyl ether 3 times. The copolymer was dried in a vacuum oven at 50 °C for 24 hours and the molecular weight was determined by end group analysis of the methyl ether groups of pEGMA ( $\delta = 3.13$  ppm, 3 H). The % conversion were determined by analysis of the reaction mixture before and after heating.

### **3.3 Micelle Formation and Characterization**

#### **3.3.1 Micelle Formation**

Micelles were formed by the direct dissolution method. pLA-*b*-pEGMA copolymer (20 mg) was dissolved in acetone (2 mL) following drop-wise addition into purified water (4 mL) under constant stirring. The solution was left uncovered to stir for 24 hours to remove the acetone. Micelles were filtered through a 0.2  $\mu\text{m}$  nylon filter prior to use.

#### **3.3.2 Dynamic Light Scattering (DLS) and Zeta Potential**

The hydrodynamic diameter of the micelles was determined using a Brookhaven 90Plus particle analyzer running Particle Solutions Software (Version 2.6, Brookhaven Instruments Corporation) equipped with a 659 nm laser and a 90 degree detection angle. DLS measurements were carried out at 25 °C and performed at a count rate between 200-500 kilocounts/s. The average of three samples with ten runs each is reported.

Zeta potential was measured using a ZetaPlus zeta potential analyzer (Brookhaven Instrument Corporation) operating in PALS (phase analysis light scattering) mode in polystyrene cuvettes. Samples were prepared in 10 mM NaCl and the average of 2 individual samples, prepared under the same conditions with 15 cycles each is reported.

### **3.3.3 Transmission Electron Microscope (TEM)**

TEM images were obtained with a Joel JEM-1200EX transmission electron microscope with an 80 kV electron beam. Samples were prepared by placing 3  $\mu\text{L}$  of 100  $\mu\text{g}/\text{mL}$  micelle solution on a 200 mesh Formvar-coated copper grid. The water was allowed to evaporate at room temperature prior to imaging.

### **3.3.4 Critical Micelle Concentration (CMC)**

Critical Micelle Concentrations were determined using the standard pyrene fluorescent probe method. Briefly, 4  $\mu\text{L}$  of pyrene solution (100  $\mu\text{g}/\text{mL}$  in acetone) was added into 2 mL vials and allowed to evaporate overnight to form a pyrene film. 1 mL of micelle solution (ranging from  $10^{-5}$  mg/mL to 1 mg/mL) was added into each vial resulting in final pyrene concentrations of 2  $\mu\text{M}$ . The solutions were incubated for 24 hours at room temperature while shaking. The fluorescence intensity was measured using a Tecan Infinite M1000 Pro fluorescent plate reader (Männedorf, Switzerland) with an excitation wavelength of 340 nm and emission wavelength of 373 and 383 nm (bandwidth of 5 nm). The CMC was determined by plotting the intensity ratio (373/383) against the logarithm of concentrations.

### **3.4 Cyclosporine A Loaded Micelles and Release**

Cyclosporine A loaded micelles were prepared similarly to the micellization procedure as described above with the addition of dissolving CycA (3 mg) into the polymer:acetone solution. Free CycA which is poorly soluble in water and forms aggregates, was removed through

filtration (0.2  $\mu\text{m}$  nylon filter) and the filtrate was collected to determine the entrapment efficiency. 1 mL of sample was then added to 3.5 kDa MWCO dialysis tubes and placed in 30 mL of simulated tear film (STF). STF is comprised of NaCl (6.7 mg/mL),  $\text{NaHCO}_3$  (2 mg/mL) and  $\text{CaCl}_2 \cdot 2\text{H}_2\text{O}$  (0.08 mg/mL). Drug release was measured at specific time points where 1 mL of sample was removed and replaced with 1 mL of STF. These samples were analyzed using a Waters HPLC (2707 autosampler, 2489 UV spectrophotometer, 1525 binary HPLC pump, and Breeze 2 software) with a 0.7 mL/min isocratic flow rate of 75:25 acetonitrile: 0.1% trifluoroacetic acid in purified water as the mobile phase, a 60 °C column temperature, a 20  $\mu\text{L}$  sample injection volume and a 210 nm detection wavelength. A standard calibration curve for CycA (3.125-100  $\mu\text{g/mL}$ ) was used to determine the sample concentrations.

### **3.5 Preparation of Artificial Mucus and Characterization**

#### **3.5.1 Artificial Mucus**

Artificial mucus was prepared from previously published protocols with slight modifications. 5 mg/mL of pig gastric mucin type III and 1 mg/mL of guar gum were stirred and dissolved in STF for 24 hours at room temperature. The samples were stored at 4°C and used immediately within 1 week of preparation.

#### **3.5.2 Rheological Measurements**

Rheological characterization of artificial mucus was performed with a Discovery HR-2 TA instrument configured to operate with 25 mm parallel plates. 1 mL of artificial mucus was loaded and as the gap between the plates was reduced to 0.15 mm, excess mucus was removed. A frequency flow spanning 0.1 to 100  $\text{s}^{-1}$  was performed and the viscosity was estimated using a Newtonian fluid model.

### 3.6 Micelle Transport Rates in artificial mucus with MPT

MPT measurements were done using a Convex Lens-Induced Confinement (CLiC) system (ScopeSys, Montreal, Canada), where  $\sim 5 \mu\text{L}$  of micelle solution is injected into a custom-made microfluidic device with a  $10 \mu\text{m}$  thick chamber. After optimizing the concentration of the sample to achieve distinguishable, single-molecule emissions, the samples were imaged with a Leica CTR6000 inverted fluorescence microscope, using a Leica  $60\times$ , oil-immersion objective with a numerical aperture of 1.45. The micelles were excited with a 561 nm laser at 70% in widefield, epifluorescence mode. The emission light was separated from the excitation light by a multiline dichroic mirror and filtered through a 561/40 nm colour filter before being detected by an iXon Ultra DU-897U camera in single-molecule mode (17 MHz readout mode,  $3.30 \mu\text{s}$  vertical clock speed, electron-multiplying mode), a binning mode of 1 and a projected pixel size of 160 nm. The lens of the CLiC system was depressed until the top and bottom coverslips were approximately  $8 \mu\text{m}$  apart, and the sample was focused at the middle of the chamber. A 3000-frame movie was acquired with an exposure time of 10 ms and inter-frame interval of 34.6 ms. Single-molecule localization and tracking analysis was performed using the ImageJ plugin Trackmate, with a size threshold of 10 pixels. Depending on the brightness of the micelles in each sample, the quality threshold was set to 10 – 15. Using a custom-made MATLAB code, the diffusion coefficient was extracted from the tracks through the y-intercept of the linear regression fitted on a double-log mean squared displacement (logMSD) graph. Only tracks that were at least 10 frames long and had a regression  $R^2$  value of at least 0.95 were kept.

### **3.7 Statistical Analysis**

The method selected for the small sample sizes was *t* test for comparing two means. P values were obtained using paired *t*-tests in order to determine the significance of the results. All error bars represent standard deviation.

## CHAPTER 4. RESULTS AND DISCUSSION

### 4.1 Copolymer Characterization

The reaction scheme for the polymer synthesis is shown in Figure 1. The structure of the copolymer, determined by  $^1\text{H}$  NMR is shown in Figure 2. The disappearance of the PEGMA monomer peaks at 5.5 and 6 ppm, and the emergence of a novel peak at 0.8 ppm, corresponding to polymerized PEGMA (highlighted in red) is indicative of a successful reaction.

The reaction conversion was determined from comparing the alkene peaks in the  $^1\text{H}$  NMR spectra of the reaction at  $t=0$  and 24 hrs. (Figure 3). By normalizing the integration values to the peak at 5 ppm (PLA) we can determine the actual molar feed ratios of the reactants. Therefore, the reaction conversion ( $x$ ) can be determined from Equation 1.

$$\text{Equation 1.} \quad x = \left(1 - \frac{PEGMA_{final}}{PEGMA_{initial}}\right) * 100$$

The actual molar feed ratios were consistent to the theoretical and the molecular weights were subsequently calculated from the conversion. Alternatively, the molecular weight can be determined from the purified spectra (Figure 2) by integrating the peak at 3.13 ppm (highlighted in green) which corresponds the methylene peaks of PEGMA. The two methods of calculating the molecular weights produced similar values although the reaction conversion method overestimated the molecular weight due to side reactions and impurities. The reaction conversions and polymer molecular weights are summarized in Table 1.

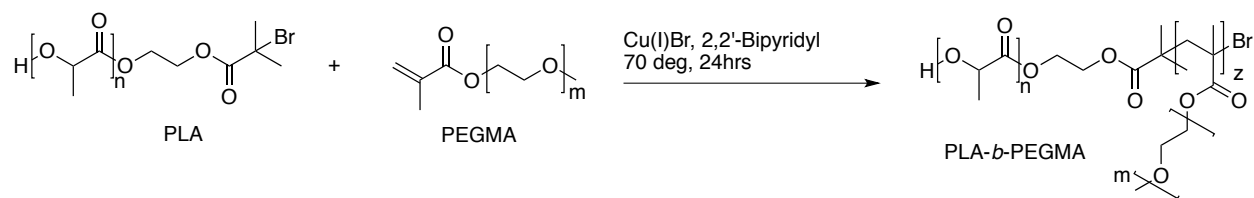


**Figure 1.** Synthesis of PLP polymers. ATRP of 2-bromoisobutryl terminated PLA as a macroinitiator with PEGMA monomer produces a diblock copolymer consisting of a hydrophobic pLA and hydrophilic pEGMA block, respectively.

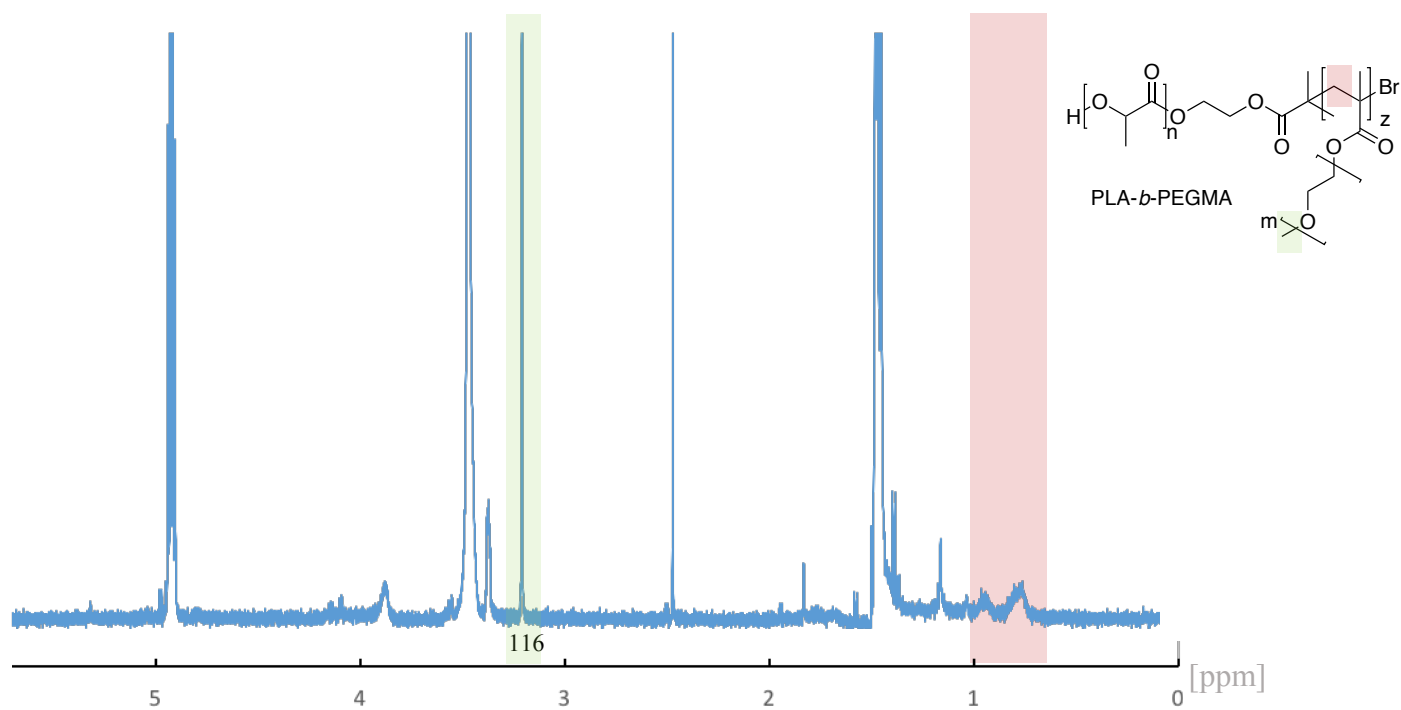


**Figure 2.**  $^1\text{H}$  NMR spectra of the purified PL5P19 copolymer.

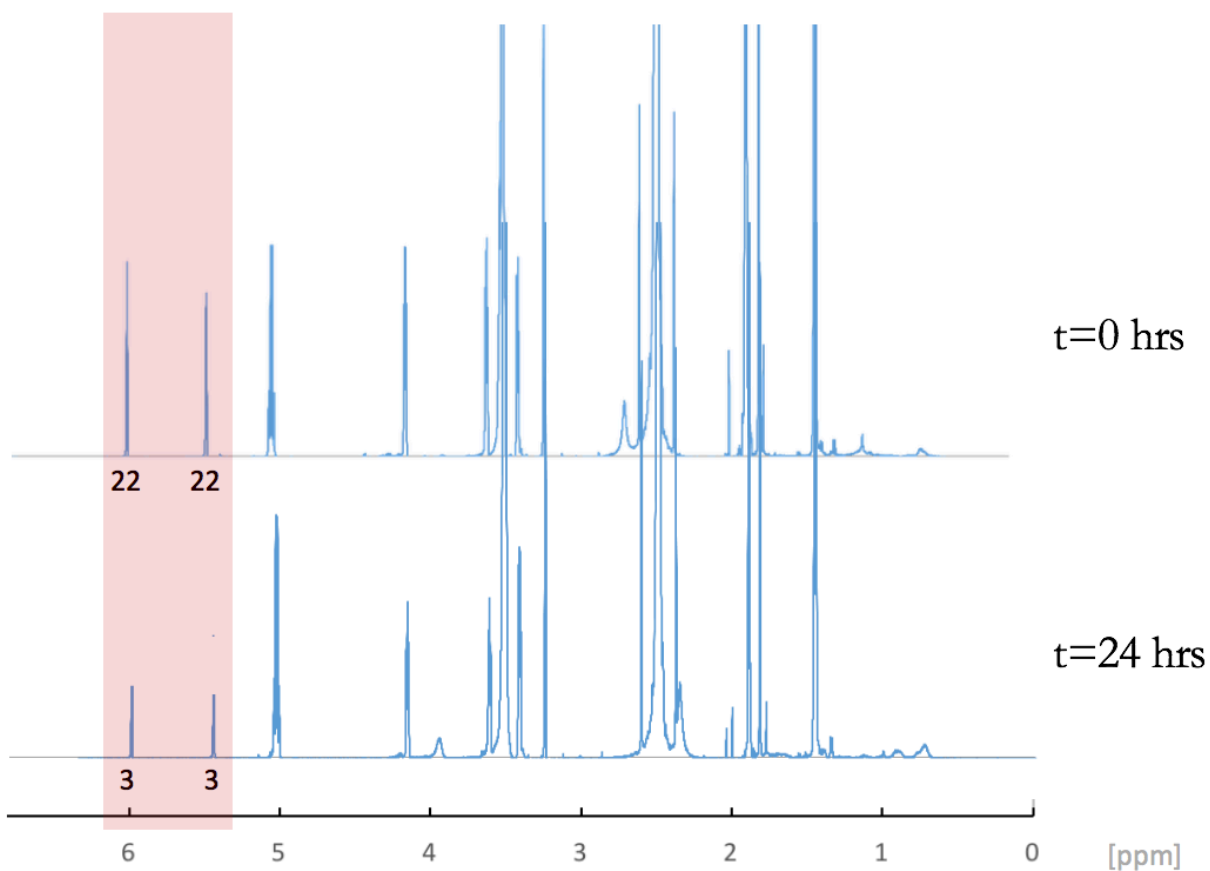


**Figure 3.**  $^1\text{H}$  NMR spectra of the reaction mixture at  $t=0$  hrs. (top) and  $t=24$  hrs. (bottom).

**Table 1.** PLP polymerization data from  $^1\text{H}$  NMR.

Polymer	$M_n$ $_{PLA}$	PEGMA <sub>initial</sub>		PEGMA <sub>final</sub>	Polymer composition
		$t=0$	x	Determined from PEG-M(3.1ppm)	
PL10P5	10,000	13	76%	9.9	PLA <sub>10k</sub> PEGMA <sub>5k</sub>
PL10P7	10,000	17	82%	14	PLA <sub>10k</sub> PEGMA <sub>7k</sub>
PL10P10	10,000	25	80%	20	PLA <sub>10k</sub> PEGMA <sub>10k</sub>
PL10P20	10,000	44	86%	38	PLA <sub>10k</sub> PEGMA <sub>20k</sub>
PL5P5	5,000	11	86%	9.5	PLA <sub>5k</sub> PEGMA <sub>5k</sub>
PL5P9	5,000	22	81%	18	PLA <sub>5k</sub> PEGMA <sub>9k</sub>
PL5P19	5,000	45	86%	38.6	PLA <sub>5k</sub> PEGMA <sub>19k</sub>

## 4.2 Micelle Morphology

Micelle z-average diameter and dispersity was determined using DLS (Table 2). Sizes of the micelles were observed to range from 60-120 nm, indicative of a trend between PEGMA content and micelle size. Micelles containing a higher PEGMA content show a higher z-average diameter by DLS. This can be explained by the balance of hydrophobic and hydrophilic components (PLA:PEGMA ratio) as well as the PLA and PEGMA block lengths.<sup>1</sup> In general, the PL10 series exhibited larger micelle size due to the larger PLA block lengths. As the PEGMA chain length and PLA:PEGMA block ratio increased, so did micelle size due to increased water content in the micelle corona. On the other hand, the size of CycA loaded PL10 series of micelles was significantly smaller than that of unloaded micelles, indicating strong hydrophobic interactions between PLA and CycA. The polydispersity of the micelles ranged from 0.126-0.298, which can be regarded as an acceptable narrow size distribution.<sup>2</sup>

**Table 2.** PLP micelle size from DLS.

Polymer	Free micelles		CycA loaded micelles	
	Size (nm)	Polydispersity	Size (nm)	Polydispersity
PL10P5	70.33 ± 0.63	0.243	51.08 ± 0.52	0.241
PL10P7	73.94 ± 0.52	0.231	68.46 ± 0.26	0.134
PL10P10	79.33 ± 0.72	0.149	74.78 ± 0.81	0.142
PL10P20	119.83 ± 2.77	0.186	84.59 ± 0.76	0.236
PL5P5	67.09 ± 0.57	0.248	68.23 ± 0.62	0.177
PL5P9	66.09 ± 0.73	0.126	66.15 ± 0.81	0.285
PL5P19	94.16 ± 1.50	0.254	67.12 ± 0.83	0.292

TEM images showed micelles that were relatively monodispersed and of spherical morphologies (Figure 4). Micelles tend to aggregate during dehydration but this effect was not seen due to the high PEG density of the micelles and the low concentrations used to prepare the samples.<sup>3</sup>

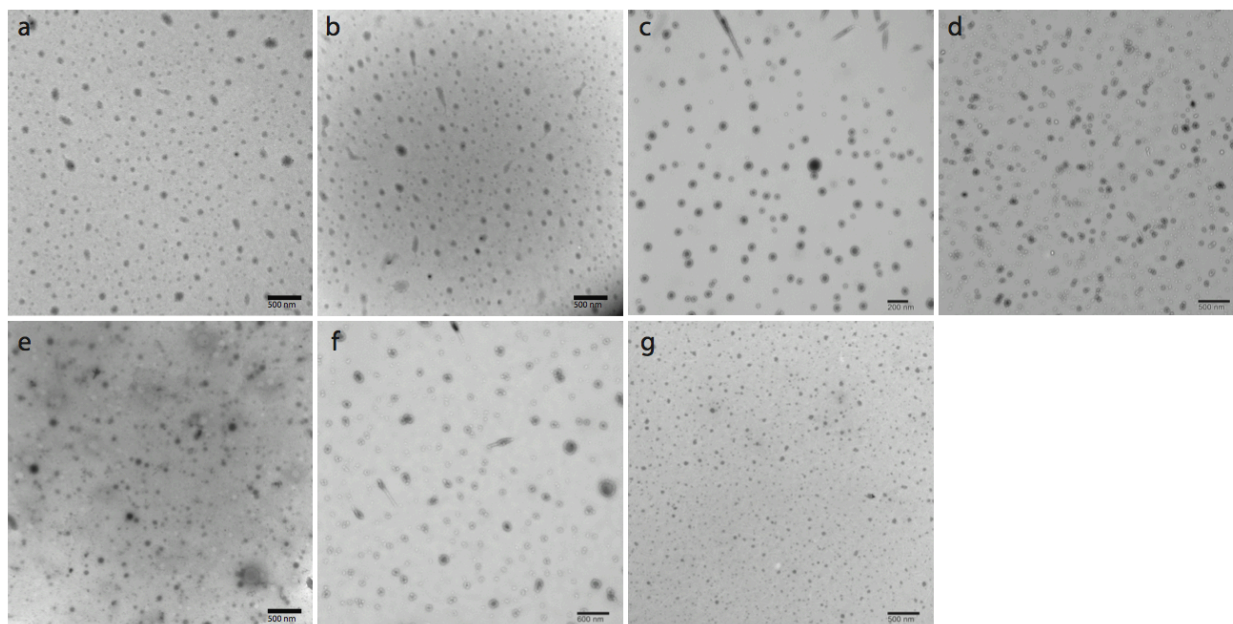


**Figure 4.** Transmission Electron Micrograph images of the pLA-*b*-pEGMA micelles. (a-d) PL10 series: (a)P5, (b)P7, (c)P10, (d)P20. (e-g) PL5 series: (e)P5, (f)P9, (g)P19.

The zeta potentials of the micelles are shown in Figure 5 and Table 3. All measurements were under -10 mV indicative of a near neutral surface. This was expected because methyl ether terminated PEGMA is a neutral polymer and PLA is a near neutral polymer with a terminal hydroxyl group. With increasing PEG density, the few hydroxyl groups that contribute to the negative charge are better shielded. However, this phenomenon is negligible since both polymers are expected to be neutral.

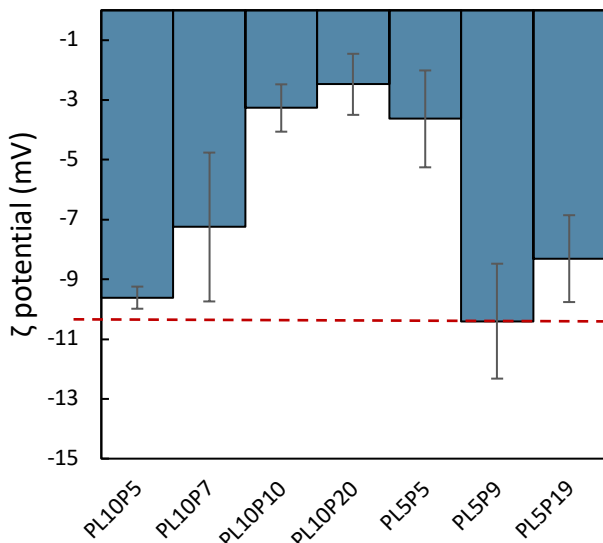


**Figure 5.** Zeta potential of PLP micelles with increasing pEGMA content. All measurements were prepared in 10 mM NaCl.

**Table 3.** PLP micelle  $\zeta$  potential and CMC

Polymer	$\zeta$ potential	CMC (mg/L)
PL10P5	$-9.61 \pm 0.37$	11.26
PL10P7	$-7.25 \pm 2.49$	12.54
PL10P10	$-3.27 \pm 0.79$	15.01
PL10P20	$-2.48 \pm 1.02$	24.67
PL5P5	$-3.63 \pm 1.62$	23.53
PL5P9	$-10.74 \pm 1.92$	24.7
PL5P19	$-8.31 \pm 1.45$	30.14

The minimum polymer concentration required to form micelles was determined using the pyrene 1:3 ratio method. The CMC's of the polymers, summarized in Table 3, ranged from 11-30 mg/L, with high PEGMA density polymer having the highest CMC (Figure 6). The increasing trend between PEGMA chain length and CMC can be explained by copolymer solubility and micelle stability. As PEGMA density increases, the hydrophilicity increases and the polymer becomes more water soluble, which increases the driving force for it to enter into solution. The PL10 series had lower CMC's even when the total molecular weights were the same (PL10P5 vs PL5P9), suggesting that micelle thermodynamic stability is governed by hydrophobic

interactions within the core of our micelles rather than the hydrophilic corona. This has been shown in PLA-PEG linear copolymers with the dominant factor on the CMC being the hydrophobic block length and that increasing the hydrophilic block also increases the CMC.<sup>4,5</sup>

The CMC of a copolymer gives an indication of the thermodynamic stability of the micelle. This is very important for topically administered ophthalmic formulations because lacrimal drainage and tear dilution increases the chances of premature drug release.<sup>6</sup> The CMC of our polymers was observed to be higher than other linear PLA-PEG block copolymers. This difference can be explained by the bottle brush nature of our polymer and how steric hindrance may influence the stability of the system.<sup>7</sup> In comparison with other PEGMA bottle brush copolymers, our CMC was 10 times lower than PEGMA-PCL copolymers reported by Taipaleenmaki et al. and 3 times lower than that of PEGMA-PLA-PEGMA micelles reported by Bakkour et al., illustrating the high stability of our formulations.<sup>8,9</sup> The low CMC demonstrates the strong tendency of our copolymers to form micelles, which is of major importance for the stability of micelles in the tear film after topical administration.

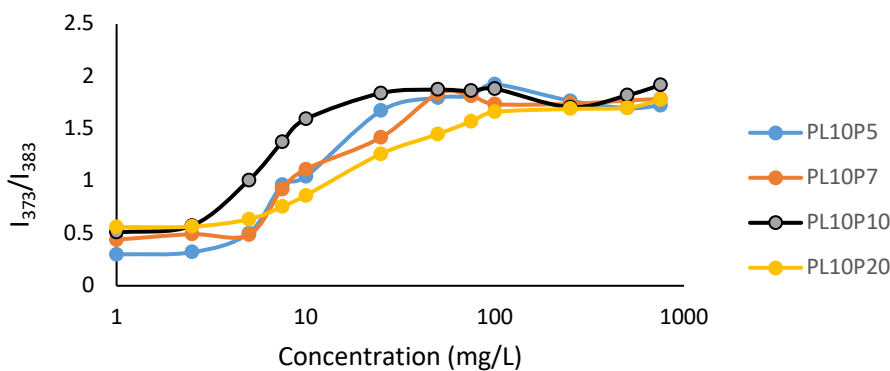


**Figure 6.** Critical Micelle Concentration of the PLP micelles determined by the pyrene fluorescence method.

### **4.3 Rheological Characterization of artificial mucus**

Mucus comprises of water, glycoproteins, lipids, salts, free proteins and displays different properties depending on its location. Therefore, it was important to design a mucus model that was representative of the tear film of the eye. There are various models of mucus described in the literature with the simplest being mucin solutions reconstituted with different solutes.<sup>10</sup>

Numerous published protocols have reported diffusive studies in mucin solutions prepared from porcine gastric mucin.<sup>8, 11, 12, 13</sup> However, those studies were not targeting the ocular mucosa and so modifications were implemented to stimulate the eye. Various concentrations (1, 5, 10, 15 mg/mL) of dried porcine gastric mucin (PGM) were added to solutions of STF containing NaCl, NaHCO<sub>3</sub>, and CaCl<sub>2</sub>•2H<sub>2</sub>O. Guar gum (1 mg/mL) is added to give the system viscoelastic properties similar to those of fresh tear film. It was determined that the sample containing 5 mg/mL of PGM had a viscosity of 34 mPa•s which was similar to the viscosity of the tear film in dry eye patients.<sup>14</sup> As a result, this recipe was used to further evaluate the mucopenetrating properties of micelles.

### **4.4 Cyclosporine A Release**

The entrapment efficiencies of the CycA loaded micelles are shown in Figure 7. All PLP micelles showed EEs greater than 60%, with PL10P5 having the highest EE of 83%. This shows that PLP micelles are very efficient at entrapping CycA and significantly improves its solubility.

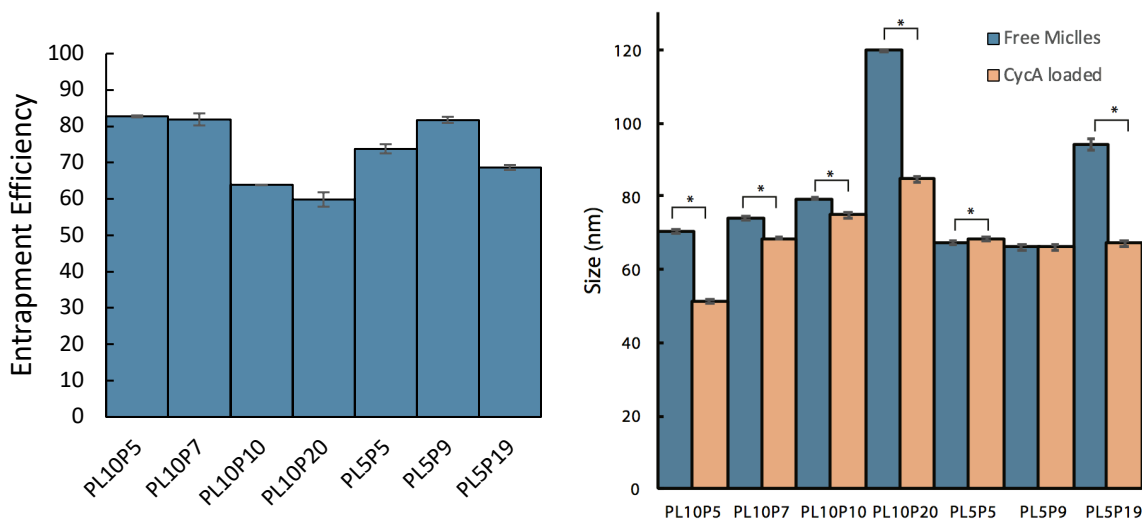


**Figure 7.** Entrapment Efficiencies of PLP polymers and its effects on micelle Size. \* $p < 0.05$  compared to free micelles.

The size of the drug loaded micelles were significantly smaller than the unloaded state due to increased hydrophobic interactions within the micelle core. This is a known effect of drug loading on micelles and further confirms that hydrophobicity increases stability from CMC experiments.<sup>15</sup>

Figure 8 shows the *in vitro* CycA release profile of PLP polymeric micelles compared with free CycA and commercially available Restasis®. Free CycA released 100% of its contents within 24 hours, illustrating that micelles significantly reduce the burst phase of a drug. Restasis® is emulsion based and improved release to 6 days but started plateauing after 1 day. In contrast, the micelles continuously released the drug for ~15 days before any plateauing effects occurred. PLP micelles maintained drug release for up to 30 days which is significantly higher than other types of CycA loaded nanocarriers for topical ocular delivery.<sup>11, 15, 16, 17</sup> This can be attributed to the high stability of the micelles which were shown to be stable over the course of 2 months. One method of sustaining even longer drug release would be chemically linking CycA to the polymer backbone. Even without chemical conjugation, our micelle drug releases were similar to chemically conjugated systems.<sup>18</sup>

Drug release from the two series of copolymers showed a two-phase release profile characterized by an initial burst phase of 24 hours, followed by a slow second non-linear diffusional release. Biphasic release profiles have often been observed in nanocarriers containing PLA. The initial burst phase of 12-20% release is likely due to freely suspended non-encapsulated CycA. Data from the free CycA release is consistent with this observation where it takes 24 hours for free Cyc to partition across the dialysis membrane. Another possible explanation is due to low drug-core compatibility and the localization of CycA outside the micellar core.<sup>19, 20</sup> The burst effect was significantly reduced in the PL10 series, illustrating that increasing PLA content strengthens the hydrophobic interactions between drug and copolymer and the localization of drug in the core, diminishing the burst effect of drug. However, the higher EE% of the PL10 series suggests that non-encapsulated CycA is the primary reason for the burst and that the reduced burst effect is due to decreased free CycA. Compared to PEG-PLA-PCL micelles synthesized by Soleymani et al., it was demonstrated that incorporating a third hydrophobic PCL block inhibits burst release. Similarly, incorporation of a middle block with poor CycA solubility may act as a physical barrier to prevent the initial burst release.

The second phase of the release profile is diffusion dependent with polymer erosion playing a role later. It was hypothesized that increasing the PEGMA content could delay drug release by increasing the diffusion distance to the micelle surface but the opposite was observed. Increasing PEGMA chain length in both PL10 and PL5 series increased the drug released possibly due to 1.) incorporation of more drug in the corona and 2.) increased rate of micelle dissociation. CMC data is consistent with this observation and suggests that increasing rate of micelle dissociation is the more plausible explanation. The increased stability of the PL10 series of polymers allows them to achieve a slower burst and more controlled drug release. For

example, between PL5P9 and PL10P5, PL5P9 started plateauing after 10 days whereas PL10P5 reached the same %CycA release after ~25 days. Enhancing the hydrophobicity and rigidity of the micellar core limits the movement of water and free ions to the core which in turn sustains or delays drug release from the carrier.<sup>6</sup> Alternatively, incorporating hydrophilic groups to the core may be an avenue to provide a pulsed mode of drug delivery. The ability to control different drug release profiles with micelles can be used to target specific ocular diseases.

Interestingly, only a maximum release of 60% of the encapsulated drug is reached. It is suspected that either CycA is trapped within the PLA core and is only released following polymer erosion and micelle dissociation, or drug degradation is occurring. Xu et al. examined the stability of CycA in dissolution media at 37 °C and determined that CycA degradation followed zero-order kinetics with a rate constant of -3.5%.<sup>21 22</sup> Similar to our observations, no other peaks other than the CycA peak was observed from the drug release studies. Results from other NP drug release studies also indicate the failure to recover 100% of the drug due to the instability of drug in release medium.<sup>23</sup> Therefore, the results from the release studies underestimate CycA release and the capabilities of micelles in delivering therapeutic agents. This highlights the importance of tailoring the therapeutic agent to the right delivery vehicle since drug delivery systems are limited to the drug lifetime.

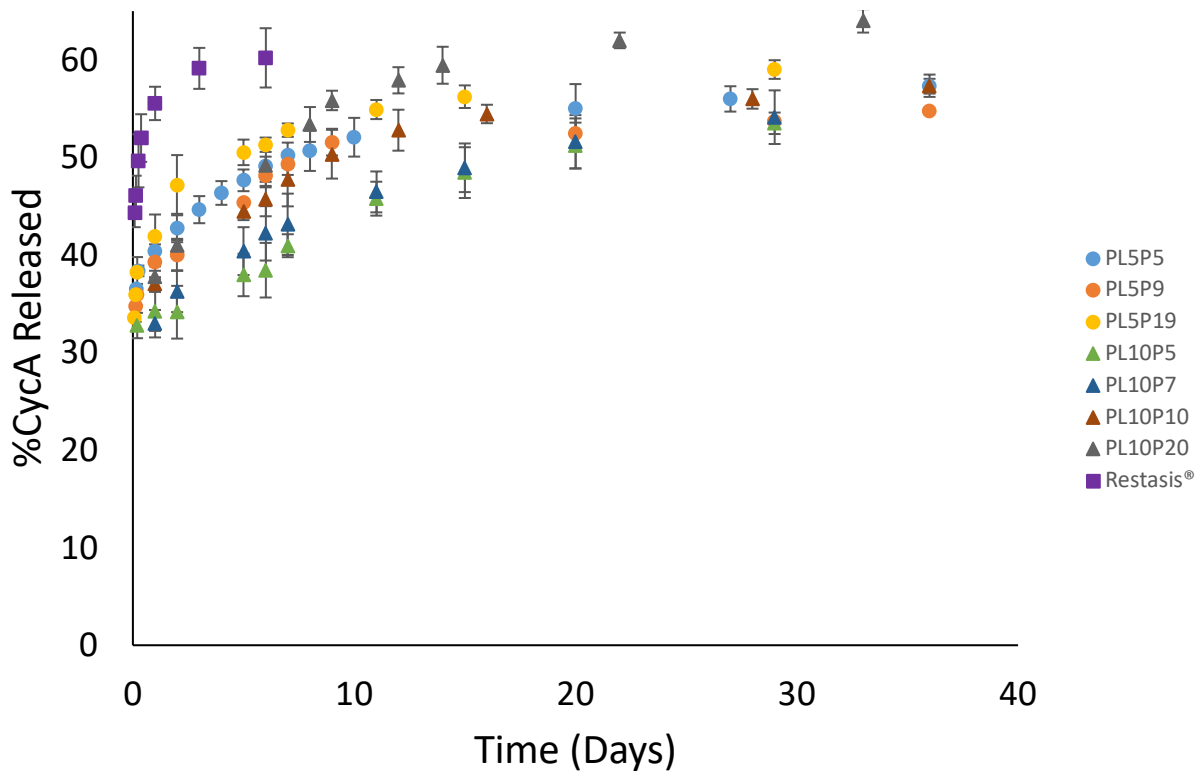


**Figure 8.** Cumulative CycA release from PLP micelles under sink conditions.

#### 4.5 MPT and Mucopenetration

Results from the MPT experiments in artificial mucus did not reveal any relationship between our micelles and mucopenetration (Figure 9, Table 4). It was hypothesized that forming micelles with a bottle brush copolymer would enhance mucopenetrating properties and that increasing pEGMA chain length would determine to what extent the relationship holds true. Unfortunately, no comparable data from the MPT experiments were obtained for numerous reasons. The negative control of our experimental design behaved more of a positive control. Phenyl Boronic Acid (PBA) based micelles were supposed to have significantly lower diffusion coefficient ratios due to their mucoadhesive nature. Instead, its value was greater than most of our micelles except for samples PL10P7 and PL5P19. Compared to literature values, mucoadhesive or obstructed particles were observed to have diffusion coefficient ratios in the  $10^{-1}$

$4 \cdot 10^{-5}$  range, whereas mucopenetrating particles values were similar to our data.<sup>24 25</sup> These results indicate that our model mucus is not ideal for mucopenetrating studies. The mucin concentrations in our model were designed to stimulate the tear film of the eye but they need to be increased in order to observe significant differences between water and mucus diffusion coefficients. Mucus is a complex biological material and it is difficult to reconstitute the complete structure of native mucus. Hanes et al. performed MPT studies in cervical vaginal mucus collected from women with normal vaginal flora.<sup>26</sup> Unfortunately, there have been no previous reports of collecting human ocular mucus but this may be an avenue of future research. Another factor that would improve the experimental results is the incorporation of brighter dyes. Nile red has half the quantum yield and absorption coefficient than BODIPY, resulting in quarter the light intensity.<sup>27</sup> Furthermore, BODIPY is more lipophilic than NR so higher encapsulation efficiency's means less dye is required. Background fluorescence was also another issue that biased our measurement's to only big, slow and bright particles. The incorporation of brighter dyes would increase the number of observable particles to obtain better particle tracks.

MPT was shown to accurately analyze the diffusion coefficients of our micelles. Comparing water diffusion coefficients obtained from DLS, the two methods produced values that were of the same order of magnitude (Table 4). However, DLS measures the diffusion of all particles and the presence of large aggregates may compromise the accuracy of the measurements.<sup>28</sup> We have demonstrated that that our technique is more suitable to characterize the diffusion coefficients of only micelles but further improvements in mucus composition are required. Despite the fact that no conclusions could be made, the high pEGMA brush density and small sizes of our micelles compared to other mucopenetrating systems suggests that our micelles still have mucopenetrating properties.

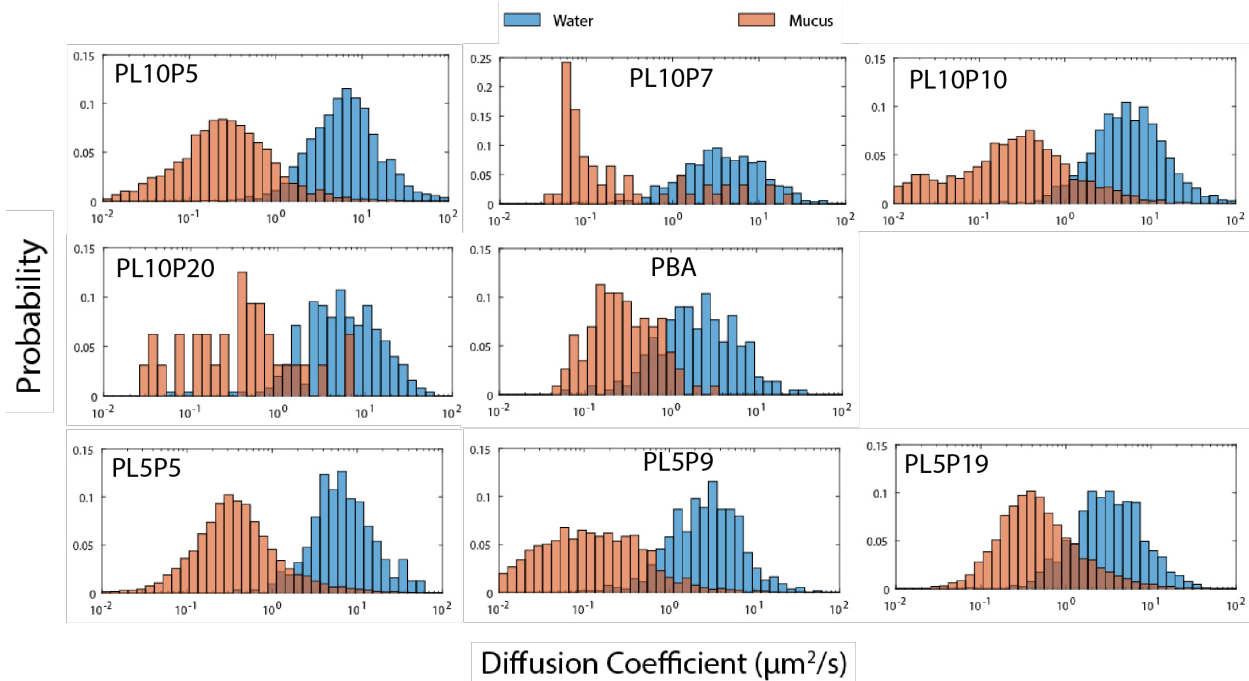


**Figure 9.** Distributions of the logarithms of individual particle diffusion coefficients in water and mucus.

**Table 4.** Diffusion Coefficients ( $\mu\text{m}^2/\text{s}$ ) and ratio

Polymer	Water		Mucus ( $D_m$ )	Ratio( $D_m/D_w$ )
	MPT ( $D_w$ )	DLS		
PL10P5	9.43	6.94	0.597	0.063
PL10P7	9.72	6.53	1.47	0.152
PL10P10	8.62	6.15	0.760	0.088
PL10P20	8.37	5.75	0.856	0.102
PL5P5	10.04	7.29	0.926	0.092
PL5P9	4.11	8.01	0.366	0.089
PL5P19	4.73	7.16	1.00	0.212
PBA	3.39	4.42	0.410	0.120

## CHAPTER 5. CONCLUSIONS

In conclusion, micelles as drug delivery vehicles have the potential to increase bioavailability and therapeutic efficacy of topically applied drugs. We have synthesized a series of poly(L-lactide)-*b*-poly(ethylene glycol methacrylate) block copolymer micelles by atom transfer radical polymerization. These micelles were confirmed by DLS and zeta potential to range in size between 60-120nm with a near neutral surface charge. TEM images showed that all micelles were relatively monodispersed and of spherical morphology. Compared to other PEGMA bottle brush copolymers, our micelles exhibited much lower critical micelle concentrations illustrating the high stability of our formulations. These micelles were shown to improve the delivery of Cyclosporine A *in vitro* compared to free drug solutions and the commercially available formulation Restasis<sup>®</sup>. This would decrease the dosage, frequency and also the systemic effects associated with current topical drops.

PLP micelles improved drug solubility and the release kinetics of hydrophobic drugs, illustrating that these materials have the potential to improve topical drug delivery. However, further studies are required to demonstrate clinical relevance. Specifically, future experiments should be focused on improving mucopenetration experiments. Precise and accurate diffusion coefficients must be measured prior to preclinical studies with rabbit models. Drug permeation studies on corneal tissues can provide insight to the effect of bottle brush polymers on permeation rate and *in vivo* studies with rabbit models can measure the ocular bioavailability. This would determine if our micelles are capable of penetrating the mucus layer to reach the underlying epithelial layers. In addition, *in vitro* experiments with human corneal epithelial cells should be conducted to determine the toxicity of our materials. It is suspected that the metal catalyst may be present in trace amounts which could have negative impacts on the eye. The

current results can also be improved with additional experiments. Polymer dispersity and molecular weights can be determined on gel permeation chromatography, micelle formulations can be improved by increasing drug loading efficiency and CycA degradation should be analyzed to fully understand the drug release kinetics. LMP micelles were demonstrated to have the potential of increasing bioavailability and therapeutic efficacy of topically applied drugs. This would help to decrease the dosage, frequency of dose, and off-target systemic toxicity that are commonly associated with topical drops.

## CHAPTER 6. REFERENCES

### Literature Review

1. Eye Anatomy: Human Eye Anatomy Diagram & Physiology | OptoPlus. Available at: <https://www.optoplus.com/en/eye-health/eye-anatomy/>. (Accessed: 29th August 2018)
2. Geroski, D. H. & Edelhauser, H. F. Drug Delivery for Posterior Segment Eye Disease. **41**, 4 (2000).
3. Gaudana, R., Ananthula, H. K., Parenky, A. & Mitra, A. K. Ocular Drug Delivery. *AAPS J.* **12**, 348–360 (2010).
4. Liu, M., Zhang, J., Shan, W. & Huang, Y. Developments of mucus penetrating nanoparticles. *Asian J. Pharm. Sci.* **10**, 275–282 (2015).
5. Thassu, D. & Chader, G. J. *Ocular Drug Delivery Systems: Barriers and Application of Nanoparticulate Systems*. (CRC Press, 2012).
6. DelMonte, D. W. & Kim, T. Anatomy and physiology of the cornea. *J. Cataract Refract. Surg.* **37**, 588–598 (2011).
7. Rehman, I. & Bhimji, S. S. Anatomy, Head, Eye. in *StatPearls* (StatPearls Publishing, 2018).
8. Asakura, T. & Shichi, H. Cytochrome P450-mediated prostaglandin  $\omega$ -1 hydroxylase activities in porcine ciliary body epithelial cells. *Exp. Eye Res.* **55**, 377–384 (1992).
9. Argikar, U. A., Dumouchel, J. L., Dunne, C. E. & Bushee, A. J. Ocular non-P450 oxidative, reductive, hydrolytic, and conjugative drug metabolizing enzymes. *Drug Metab. Rev.* **49**, 372–394 (2017).
10. Chiang, B., Jung, J. H. & Prausnitz, M. R. The suprachoroidal space as a route of administration to the posterior segment of the eye. *Adv. Drug Deliv. Rev.* **126**, 58–66 (2018).
11. Ehrlich, R., Harris, A., Wentz, S. M., Moore, N. A. & Siesky, B. A. Anatomy and Regulation of the Optic Nerve Blood Flow☆. in *Reference Module in Neuroscience and Biobehavioral Psychology* (Elsevier, 2017). doi:10.1016/B978-0-12-809324-5.01301-8
12. Bringmann, A. & Reichenbach, A. Müller Cells. in *Encyclopedia of Neuroscience* (ed. Squire, L. R.) 1083–1093 (Academic Press, 2009). doi:10.1016/B978-008045046-9.01018-4
13. Farkouh, A., Frigo, P. & Czejka, M. Systemic side effects of eye drops: a pharmacokinetic perspective. *Clin. Ophthalmol. Auckl. NZ* **10**, 2433–2441 (2016).
14. Palmer, E. A. How Safe are Ocular Drugs in Pediatrics? *Ophthalmology* **93**, 1038–1040 (1986).
15. Kaur, I. P., Smitha, R., Aggarwal, D. & Kapil, M. Acetazolamide: future perspective in topical glaucoma therapeutics. *Int. J. Pharm.* **248**, 1–14 (2002).
16. Kim, S. H., Csaky, K. G., Wang, N. S. & Lutz, R. J. Drug Elimination Kinetics Following Subconjunctival Injection Using Dynamic Contrast-Enhanced Magnetic Resonance Imaging. *Pharm. Res.* **25**, 512–520 (2008).
17. Urtti, A. Challenges and obstacles of ocular pharmacokinetics and drug delivery. *Adv. Drug Deliv. Rev.* **58**, 1131–1135 (2006).
18. Ghate, D. & Edelhauser, H. F. Ocular drug delivery. *Expert Opin. Drug Deliv.* **3**, 275–287 (2006).
19. Smith, S. J., Smith, B. D. & Mohny, B. G. Ocular side effects following intravitreal injection therapy for retinoblastoma: a systematic review. *Br. J. Ophthalmol.* **bjophthalmol-2013-303885** (2013). doi:10.1136/bjophthalmol-2013-303885

20. Wilkinson, C. P. Interventions for asymptomatic retinal breaks and lattice degeneration for preventing retinal detachment. *Cochrane Database Syst. Rev.* **9**, CD003170 (2014).
21. Matyjaszewski, K. & Davis, T. P. *Handbook of Radical Polymerization*. (John Wiley & Sons, 2003).
22. Zhu, S. & Hamielec, A. Polymerization Kinetic Modeling and Macromolecular Reaction Engineering. in *Polymer Science: A Comprehensive Reference* 779–831 (Elsevier, 2012). doi:10.1016/B978-0-444-53349-4.00127-8
23. Matyjaszewski, K. Atom Transfer Radical Polymerization (ATRP): Current Status and Future Perspectives. *Macromolecules* **45**, 4015–4039 (2012).
24. Matyjaszewski, K. & Tsarevsky, N. V. Nanostructured functional materials prepared by atom transfer radical polymerization. *Nat. Chem.* **1**, 276–288 (2009).
25. Matyjaszewski, K. & Xia, J. Atom Transfer Radical Polymerization. *Chem. Rev.* **101**, 2921–2990 (2001).
26. Chiefari, J. *et al.* Living Free-Radical Polymerization by Reversible Addition–Fragmentation Chain Transfer: The RAFT Process. *Macromolecules* **31**, 5559–5562 (1998).
27. Hawker, C. J., Bosman, A. W. & Harth, E. New Polymer Synthesis by Nitroxide Mediated Living Radical Polymerizations. *Chem. Rev.* **101**, 3661–3688 (2001).
28. Talelli, M. *et al.* Core-crosslinked polymeric micelles: Principles, preparation, biomedical applications and clinical translation. *Nano Today* **10**, 93–117 (2015).
29. Aliabadi, H. M. & Lavasanifar, A. Polymeric micelles for drug delivery. *Expert Opin. Drug Deliv.* **3**, 139–162 (2006).
30. Mandal, A., Bisht, R., Rupenthal, I. D. & Mitra, A. K. Polymeric micelles for ocular drug delivery: From structural frameworks to recent preclinical studies. *J. Controlled Release* **248**, 96–116 (2017).
31. Kedar, U., Phutane, P., Shidhaye, S. & Kadam, V. Advances in polymeric micelles for drug delivery and tumor targeting. *Nanomedicine Nanotechnol. Biol. Med.* **6**, 714–729 (2010).
32. Harada-Shiba, M. *et al.* Polyion complex micelles as vectors in gene therapy – pharmacokinetics and in vivo gene transfer. *Gene Ther.* **9**, 407–414 (2002).
33. Yoo, H. S. & Park, T. G. Biodegradable polymeric micelles composed of doxorubicin conjugated PLGA–PEG block copolymer. *J. Controlled Release* **70**, 63–70 (2001).
34. Boddupalli, B. M., Mohammed, Z. N. K., Nath, R. A. & Banji, D. Mucoadhesive drug delivery system: An overview. *J. Adv. Pharm. Technol. Res.* **1**, 381–387 (2010).
35. Lai, S. K., Wang, Y.-Y. & Hanes, J. Mucus-penetrating nanoparticles for drug and gene delivery to mucosal tissues. *Adv. Drug Deliv. Rev.* **61**, 158–171 (2009).
36. Netsomboon, K. & Bernkop-Schnürch, A. Mucoadhesive vs. mucopenetrating particulate drug delivery. *Eur. J. Pharm. Biopharm.* **98**, 76–89 (2016).
37. Mucoadhesion of Polymeric Drug Delivery Systems: Polymeric Nanoparticles and its Interactions with the Intestinal Barrier. 5 (2016).
38. Sarti, F., Staaf, A., Sakloetsakun, D. & Bernkop-Schnürch, A. Thiolated hydroxyethylcellulose: synthesis and in vitro evaluation. *Eur. J. Pharm. Biopharm. Off. J. Arbeitsgemeinschaft Pharm. Verfahrenstechnik EV* **76**, 421–427 (2010).
39. Khutoryanskiy, V. V. Advances in Mucoadhesion and Mucoadhesive Polymers. *Macromol. Biosci.* **11**, 748–764 (2011).

40. Prosperi-Porta, G., Kedzior, S., Muirhead, B. & Sheardown, H. Phenylboronic-Acid-Based Polymeric Micelles for Mucoadhesive Anterior Segment Ocular Drug Delivery. *Biomacromolecules* **17**, 1449–1457 (2016).
41. Mitra, A. K. *Treatise on Ocular Drug Delivery*. (Bentham Science Publishers, 2013).
42. Taipaleenmäki, E. M., Mouritzen, S. A., Schattling, P. S., Zhang, Y. & Städler, B. Mucopenetrating micelles with a PEG corona. *Nanoscale* **9**, 18438–18448 (2017).
43. Schopf, L. R. *et al.* Topical Ocular Drug Delivery to the Back of the Eye by Mucus-Penetrating Particles., Topical Ocular Drug Delivery to the Back of the Eye by Mucus-Penetrating Particles. *Transl. Vis. Sci. Technol. Transl. Vis. Sci. Technol.* **4**, 4, 11–11 (2015).
44. Li, M., Azad, M., Davé, R. & Bilgili, E. Nanomilling of Drugs for Bioavailability Enhancement: A Holistic Formulation-Process Perspective. *Pharmaceutics* **8**, (2016).
45. Groo, A.-C. & Lagarce, F. Mucus models to evaluate nanomedicines for diffusion. *Drug Discov. Today* **19**, 1097–1108 (2014).
46. Suh, J. Real-time multiple-particle tracking: applications to drug and gene delivery. *Adv. Drug Deliv. Rev.* **57**, 63–78 (2005).
47. Shen, H. *et al.* Single Particle Tracking: From Theory to Biophysical Applications. *Chem. Rev.* **117**, 7331–7376 (2017).

## Results and Discussion

1. Somekawa, S. *et al.* Size-Controlled Nanomicelles of Poly(lactic acid)–Poly(ethylene glycol) Copolymers with a Multiblock Configuration. *Polymers* **7**, 1177–1191 (2015).
2. Zhao, J. & Feng, S.-S. Effects of PEG tethering chain length of vitamin E TPGS with a Herceptin-functionalized nanoparticle formulation for targeted delivery of anticancer drugs. *Biomaterials* **35**, 3340–3347 (2014).
3. Logie, J., Owen, S. C., McLaughlin, C. K. & Shoichet, M. S. PEG-Graft Density Controls Polymeric Nanoparticle Micelle Stability. *Chem. Mater.* **26**, 2847–2855 (2014).
4. Pourhosseini, P. S., Amani, R., Saboury, A. A., Najafi, F. & Imani, M. Effect of block lengths on the association behavior of poly(l-lactic acid)/poly(ethylene glycol) (PLA–PEG–PLA) micelles in aqueous solution. *J. Iran. Chem. Soc.* **11**, 467–470 (2014).
5. Hildgen, P., Leroux, J.-C., Zhao, Y. & Calon, F. Présentée par : Mahmoud El Sabahy. 283
6. Mandal, A., Bisht, R., Rupenthal, I. D. & Mitra, A. K. Polymeric micelles for ocular drug delivery: From structural frameworks to recent preclinical studies. *J. Controlled Release* **248**, 96–116 (2017).
7. Venkatraman, S. S., Jie, P., Min, F., Freddy, B. Y. C. & Leong-Huat, G. Micelle-like nanoparticles of PLA–PEG–PLA triblock copolymer as chemotherapeutic carrier. *Int. J. Pharm.* **298**, 219–232 (2005).
8. Taipaleenmäki, E. M., Mouritzen, S. A., Schattling, P. S., Zhang, Y. & Städler, B. Mucopenetrating micelles with a PEG corona. *Nanoscale* **9**, 18438–18448 (2017).
9. Bakkour, Y., Darcos, V., Coumes, F., Li, S. & Coudane, J. Brush-like amphiphilic copolymers based on polylactide and poly(ethylene glycol): Synthesis, self-assembly and evaluation as drug carrier. *Polymer* **54**, 1746–1754 (2013).
10. Groo, A.-C. & Lagarce, F. Mucus models to evaluate nanomedicines for diffusion. *Drug Discov. Today* **19**, 1097–1108 (2014).

11. Cheng, C., Zhang, X., Wang, Y., Sun, L. & Li, C. Phenylboronic acid-containing block copolymers: synthesis, self-assembly, and application for intracellular delivery of proteins. *New J. Chem.* **36**, 1413 (2012).
12. Burruano, B. T., Schnaare, R. L. & Malamud, D. Synthetic cervical mucus formulation. *Contraception* **66**, 137–140 (2002).
13. Dawson, M., Krauland, E., Wirtz, D. & Hanes, J. Transport of Polymeric Nanoparticle Gene Carriers in Gastric Mucus. *Biotechnol. Prog.* **20**, 851–857 (2004).
14. Tiffany, J. M. The viscosity of human tears. *Int. Ophthalmol.* **15**, 371–376 (1991).
15. Prosperi-Porta, G., Kedzior, S., Muirhead, B. & Sheardown, H. Phenylboronic-Acid-Based Polymeric Micelles for Mucoadhesive Anterior Segment Ocular Drug Delivery. *Biomacromolecules* **17**, 1449–1457 (2016).
16. Liu, S. *et al.* Phenylboronic acid modified mucoadhesive nanoparticle drug carriers facilitate weekly treatment of experimentally induced dry eye syndrome. *Nano Res.* **8**, 621–635 (2015).
17. Liu, S., Jones, L. & Gu, F. X. Development of Mucoadhesive Drug Delivery System Using Phenylboronic Acid Functionalized Poly(D, L-lactide)-*b*-Dextran Nanoparticles. *Macromol. Biosci.* **12**, 1622–1626 (2012).
18. Yoo, H. S. & Park, T. G. Biodegradable polymeric micelles composed of doxorubicin conjugated PLGA–PEG block copolymer. *J. Controlled Release* **70**, 63–70 (2001).
19. Soleymani Abyaneh, H., Vakili, M. R., Zhang, F., Choi, P. & Lavasanifar, A. Rational design of block copolymer micelles to control burst drug release at a nanoscale dimension. *Acta Biomater.* **24**, 127–139 (2015).
20. Soleymani Abyaneh, H., Vakili, M. R., Shafaati, A. & Lavasanifar, A. Block Copolymer Stereoregularity and Its Impact on Polymeric Micellar Nanodrug Delivery. *Mol. Pharm.* **14**, 2487–2502 (2017).
21. Xu, X. *et al.* Development and Validation of a HPLC Method for Dissolution and Stability Assay of Liquid-Filled Cyclosporine Capsule Drug Products. *AAPS PharmSciTech* **14**, 959–967 (2013).
22. Kumar, M., Singhal, S. K. & Singh, A. Development and validation of a stability indicating HPLC assay method for cyclosporine in cyclosporine oral solution USP. *J. Pharm. Biomed. Anal.* **25**, 9–14 (2001).
23. Abouelmagd, S. A., Sun, B., Chang, A. C., Ku, Y. J. & Yeo, Y. Release Kinetics Study of Poorly Water-Soluble Drugs from Nanoparticles: Are We Doing It Right? *Mol. Pharm.* **12**, 997–1003 (2015).
24. Wang, Y.-Y. *et al.* Addressing the PEG Mucoadhesivity Paradox to Engineer Nanoparticles that “Slip” through the Human Mucus Barrier. *Angew. Chem. Int. Ed.* **47**, 9726–9729 (2008).
25. Xu, Q. *et al.* Scalable method to produce biodegradable nanoparticles that rapidly penetrate human mucus. *J. Controlled Release* **170**, 279–286 (2013).
26. Lai, S. K., Wang, Y.-Y. & Hanes, J. Mucus-penetrating nanoparticles for drug and gene delivery to mucosal tissues. *Adv. Drug Deliv. Rev.* **61**, 158–171 (2009).
27. Martinez, V. & Henary, M. Nile Red and Nile Blue: Applications and Syntheses of Structural Analogues. *Chem. - Eur. J.* **22**, 13764–13782 (2016).
28. Filipe, V., Hawe, A. & Jiskoot, W. Critical Evaluation of Nanoparticle Tracking Analysis (NTA) by NanoSight for the Measurement of Nanoparticles and Protein Aggregates. *Pharm. Res.* **27**, 796–810 (2010).

29. Suk, J. S., Xu, Q., Kim, N., Hanes, J. & Ensign, L. M. PEGylation as a strategy for improving nanoparticle-based drug and gene delivery. *Adv. Drug Deliv. Rev.* **99**, 28–51 (2016).
30. Liu, M., Zhang, J., Shan, W. & Huang, Y. Developments of mucus penetrating nanoparticles. *Asian J. Pharm. Sci.* **10**, 275–282 (2015).
31. Aliabadi, H. M. & Lavasanifar, A. Polymeric micelles for drug delivery. *Expert Opin. Drug Deliv.* **3**, 139–162 (2006).